Mesozoic geologic evolution of the Xolapa migmatitic complex north of Acapulco, southern Mexico: implications for paleogeographic reconstructions

Rosalva Pérez-Gutiérrez[1], Luigi A. Solari[2,*], Arturo Gómez-Tuena[2], and Uwe Martens[3]

[1] Instituto de Geología, Universidad Nacional Autónoma de México, Cd. Universitaria, Del. Coyoacán, 04510 México D.F., Mexico.
[2] Centro de Geociencias, Universidad Nacional Autónoma de México, Campus Juriquilla, Blvd. Juriquilla 3001, 76230 Querétaro, Qro., Mexico.
[3] Department of Geological and Environmental Sciences, Stanford University, 450 Serra Mall, Bldg 320, Stanford, CA 94304, United States.
**solari@servidor.unam.mx*

ABSTRACT

The Xolapa Complex in the Acapulco-Tierra Colorada area, southern Mexico, is made up of orthogneisses and paragneisses, both affected by a variable degrees of migmatization. These rocks are intruded by several episodes of Jurassic-Oligocene, calc-alkaline granitic magmatism. Three phases of ductile deformation affected the gneisses and migmatites. D_1 produced an amphibolite-facies metamorphic banding (M_1) and a penetrative S_1 foliation, axial planar to isoclinal, recumbent F_1 folds with axes parallel to a NE to NW, gently plunging, L_1 stretching lineation. D_2 consists of a S_2 foliation defined by hornblende, biotite and garnet, synchronous with M2 migmatization that generated leucosomes, which are generally parallel to S_1. D_3 is made up of asymmetric, chevron F_3 folds that deform the composite S_1/S_2 foliation during greenschist to lower amphibolite metamorphism (M3). U-Pb SHRIMP (Sensitive High-Resolution Ion Micropobe) geochronology carried out on zircon separated from two orthogneisses yielded an Early Jurassic magmatic event (178.7 ± 1.1 Ma) and the age of migmatization (133.6 ± 0.9 Ma). Two episodes of Pb loss were also recognized, the first at 129.2 ± 0.4 Ma, and the second during the earliest Paleocene (61.4 ± 1.5 Ma); they are probably associated with two episodes of magmatism. The Early Jurassic magmatic arc may be correlated with a magmatic arc in the eastern Guerrero terrane. The Early Cretaceous migmatization is inferred to have resulted from shortening, possibly due to the accretion of an exotic block, such as the Chortís block along whose northern margin contemporaneous, high-pressure metamorphism has been recorded.

Key words: migmatization, U-Pb, Mesozoic, Xolapa Complex, southern México.

RESUMEN

El Complejo Xolapa es el terreno metamórfico más extenso en el sur de México. En el segmento que va de Acapulco a Tierra Colorada está constituido por ortogneises y paragneises, afectados por un grado variable de migmatización. El basamento del Complejo Xolapa está también afectado por diversos episodios de magmatismo granítico de afinidad geoquímica calcialcalina y edades que van del Jurásico al Oligoceno. Tres fases de deformación dúctil afectan los gneises y migmatitas. Un bandeamiento metamórfico se desarrolla durante D_1, y está asociado con una foliación penetrativa S_1, en facies de anfibolita, que actúa como plano axial de pliegues de recumbentes a isoclinales F_1. Una lineación de estiramiento L_1 está presente en toda el área de estudio, con buzamiento tanto al NE como NW. La

orientación de las estructuras D_1 controla el emplazamiento de los lentes de leucosoma D_2, generados durante el proceso de migmatización. Afuera de los dominios leucosomáticos, la foliación S_2 está caracterizada por la asociación hornblenda + biotita + granate. Pliegues asimétricos de tipo chevron relacionados a la fase F_3 deforman la foliación compuesta S_1/S_2, en condiciones de facies de esquistos verdes hasta anfibolita. La geocronología de U-Pb por SHRIMP (microsonda iónica de alta resolución) realizada en zircones separados de dos muestras de ortogneises permitió reconocer un evento magmático jurásico temprano (178.7 ± 1.1 Ma), así como la edad de migmatización en esta porción del complejo de Xolapa calculada en 133.6 ± 0.9 Ma. Dos episodios de pérdida de Pb se pueden reconocer en algunos de los zircones de las muestras fechadas. El primero es posterior al pico de migmatización (129.2 ± 0.4 Ma), y el segundo ocurrió durante el Paleoceno temprano (61.4 ± 1.5 Ma), y probablemente ambos son un efecto térmico asociado a dos de los episodios magmáticos posteriores. Estos datos sugieren que un arco magmático del Jurásico temprano habría constituido el basamento del Complejo Xolapa; se sugiere que este mismo arco corresponda a la porción este del terreno Guerrero, en donde algunas edades magmáticas similares han sido reportadas. La migmatización ocurrió durante el Cretácico temprano como consecuencia del acortamiento producido por la accreción de un bloque exótico. El bloque de Chortís es un candidato posible para tal colisión, ya que registra un evento metamórfico de alta presión contemporáneo con el evento de migmatización en el Complejo Xolapa.

Palabras clave: migmatización, U-Pb, Mesozoico, Complejo Xolapa, sur de México.

INTRODUCTION

High-grade metamorphic terrains form a large portion of the continental crust exposed in Phanerozoic and Precambrian orogens. Inasmuch as these kinds of metamorphic terrains represent exhumed portions of the middle and lower continental crust, understanding their geologic evolution sheds light on the deep crustal processes.

The geology of southern Mexico is composed of a mosaic of tectonostratigraphic terranes, (Figure 1) (Campa and Coney, 1983; Sedlock *et al.*, 1993; Keppie, 2004). Along the Pacific coast, the Xolapa (or Chatino) terrane, ~600 km long and ~50–80 km wide, is a composite plutonic and metamorphic terrane. The Xolapa terrane truncates the terranes exposed to the north, which consist (from W to E) of: (a) the Mesozoic Guerrero terrane (Talavera-Mendoza *et al.*, 2007; Centeno-García *et al.*, 2008), (b) the polymetamorphic, Paleozoic-bearing Mixteca Terrane (Ortega-Gutiérrez *et al.*, 1999), and (c) the Mesoproterozoic, granulite-bearing Zapoteco terrane (Keppie *et al.*, 2001; Keppie *et al.*, 2003; Solari *et al.*, 2003; Solari *et al.*, 2004). The Mixteca and Zapoteco terranes were amalgamated during the Permian, whereas the Guerrero terrane was accreted in the Mesozoic (Centeno-García *et al.*, 1993; Elias-Herrera and Ortega-Gutiérrez, 2002; Keppie, 2004; Centeno-García *et al.*, 2008). The allochthonous or autochthonous nature of the Xolapa Complex is still debated (*e.g.*, Keppie, 2004; Ducea *et al.*, 2004; Corona-Chávez *et al.*, 2006). One view suggests that the Xolapa Complex is autochthonous, originated *in situ* by thinning and reheating of the continental crust during Tertiary (*e.g.*, Herrmann *et al.*, 1994; Schaaf *et al.*, 1995; Morán-Zenteno *et al.*, 1996; Ducea *et al.*, 2004). A contrasting idea suggests that the Xolapa is allochthonous, and was accreted to the continental margin of southern Mexico during Mesozoic–Tertiary (*e.g.*, Corona-Chávez *et al.*, 2006).

In an attempt to resolve this debate, we undertook a combination of fieldwork, petrologic and geochronologic analyses to better document the sequence of tectonothermal events in the Xolapa Complex. A key question to be addressed is the timing of migmatization and high-grade metamorphism of the Xolapa Complex. Various time ranges have been proposed: Late Jurassic to earliest Cretaceous (*e.g.*, Ducea *et al.*, 2004; Solari *et al.*, 2007), Late Cretaceous to earliest Paleocene (~60–110 Ma, Corona-Chávez *et al.*, 2006), and Early Tertiary (46–66 Ma; Herrmann *et al.*, 1994). In this paper, we present detailed structural description of the Xolapa Complex north of Acapulco (Figures 1 and 2), the geochemical characteristic of some of the high-grade metamorphic rocks, and U-Pb zircon geochronology. These data are then applied to Tertiary reconstructions (*e.g.*, Solari *et al.*, 2007).

REGIONAL GEOLOGY

The Xolapa Complex is made up by a sequence of high-grade metasedimentary and metaigneous rocks that are frequently intruded by both deformed and undeformed plutonic rocks. Previous work was generally limited to either field descriptions, (*i.e.*, De Cserna, 1965), combined geochemical and geochronological analyses (Morán-Zenteno, 1992; Herrmann *et al.*, 1994; Ducea *et al.*, 2004), or combined field and petrological work without geochronology (Corona-Chávez *et al.*, 2006). As there is some confusion about what constitutes the Xolapa Complex, we define the Xolapa Complex as those rocks that are affected by migmatization and ductile deformation, which predate the intrusion and further solid-state shearing of the ~130 Ma

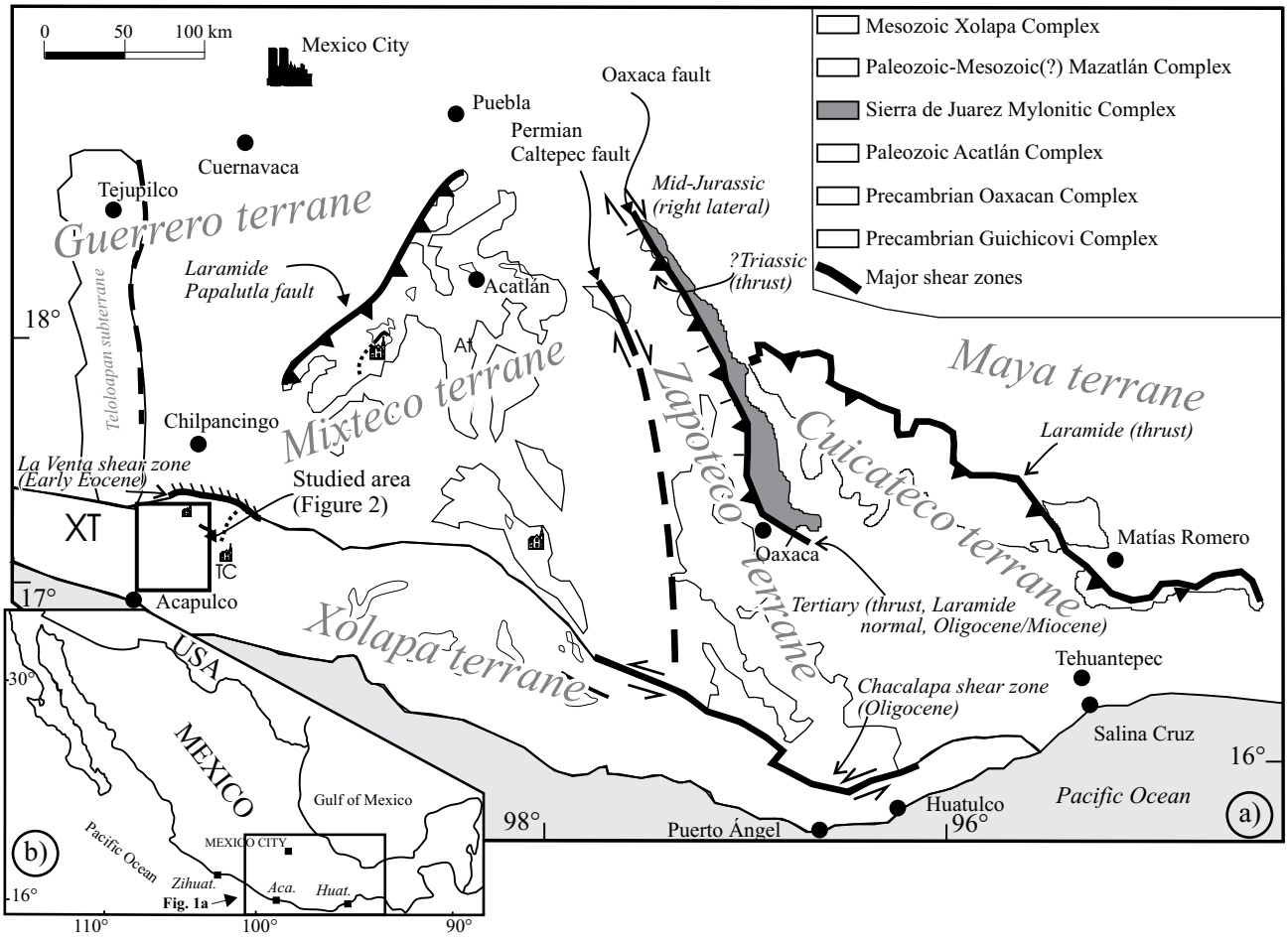

Figure 1. Simplified terrane subdivision of southern Mexico. Main basement complexes are also indicated. Modified from Solari *et al.* (2007). Terrane subdivision according to Campa and Coney (1983), Sedlock *et al.* (1993), and Keppie (2004).

deformed granites (*e.g.*, Solari *et al.*, 2007, and see below). Previous definitions of the Xolapa Complex included all the metamorphic and igneous pre-Oligocene rocks exposed in the area (*e.g.*, De Cserna, 1965; Alaniz-Álvarez and Ortega-Gutiérrez, 1997.

The northern boundary of the Xolapa terrane (Figure 1) is marked by normal and left-lateral ductile shear zones, which were active from the Eocene on the west (Tierra Colorada shear zone, Riller *et al.*, 1992; Solari *et al.*, 2007), to the Oligocene in the east (Chacalapa shear zone, Tolson, 2005). While protolith ages of the metasediments have yet to be determined, the oldest magmatic arc intruding the Xolapa Complex is documented as Jurassic to Early Cretaceous (*e.g.*, Guerrero-García *et al.*, 1978; Morán-Zenteno, 1992; Herrmann *et al.*, 1994; Ducea *et al.*, 2004). The youngest undeformed plutons intruding the Xolapa Complex range from ~34 Ma in the Acapulco – Tierra Colorada area (Hermann *et al.* 1994; Ducea *et al.*, 2004), and become younger toward SE (~25–29 Ma in Puerto Escondido – Huatulco; Hermann *et al.* 1994; Ducea *et al.*, 2004). At least two other intrusive events occurred between the oldest and youngest magmatic events. Thus, north of Acapulco, Solari *et al.* (2007) presented U-Pb concordant ages of ~129 Ma on undeformed to slightly deformed granites, and ~55 Ma ages for other granites locally affected by ductile shearing. The ~129 Ma ages are in the range of the deformed granites of Morán-Zenteno (1992), whereas the ~55 Ma ages are similar to those previously determined by Ducea *et al.* (2004) on the Acapulco syeno-granite. Geochronology of deformed samples from the Xolapa Complex indicates the presence of protoliths similar to the neighboring metamorphic complexes. For instance, north of Puerto Ángel (Figure 1) rocks have both igneous and metamorphic Grenvillian ages, similar to those in the Oaxacan Complex (*e.g.*, Keppie *et al.*, 2001; Ducea *et al.*, 2004). North of Puerto Escondido, Ducea *et al.* (2004) reported Permian ages in a biotite-bearing gneiss that are similar to ages reported in granite and granodiorite belonging to the Acatlán Complex (Yañez *et al.*, 1991; Keppie *et al.*, 2004, 2008), the Juchatengo complex (Grajales-Nishimura, 1988; Grajales-Nishimura *et al.*, 1999), and the stitching granites along the Caltepec fault zone (Elias-Herrera and Ortega-Gutiérrez, 2002). In the Acapulco transect, ages reported so far are no older than Middle Jurassic, and are similar to

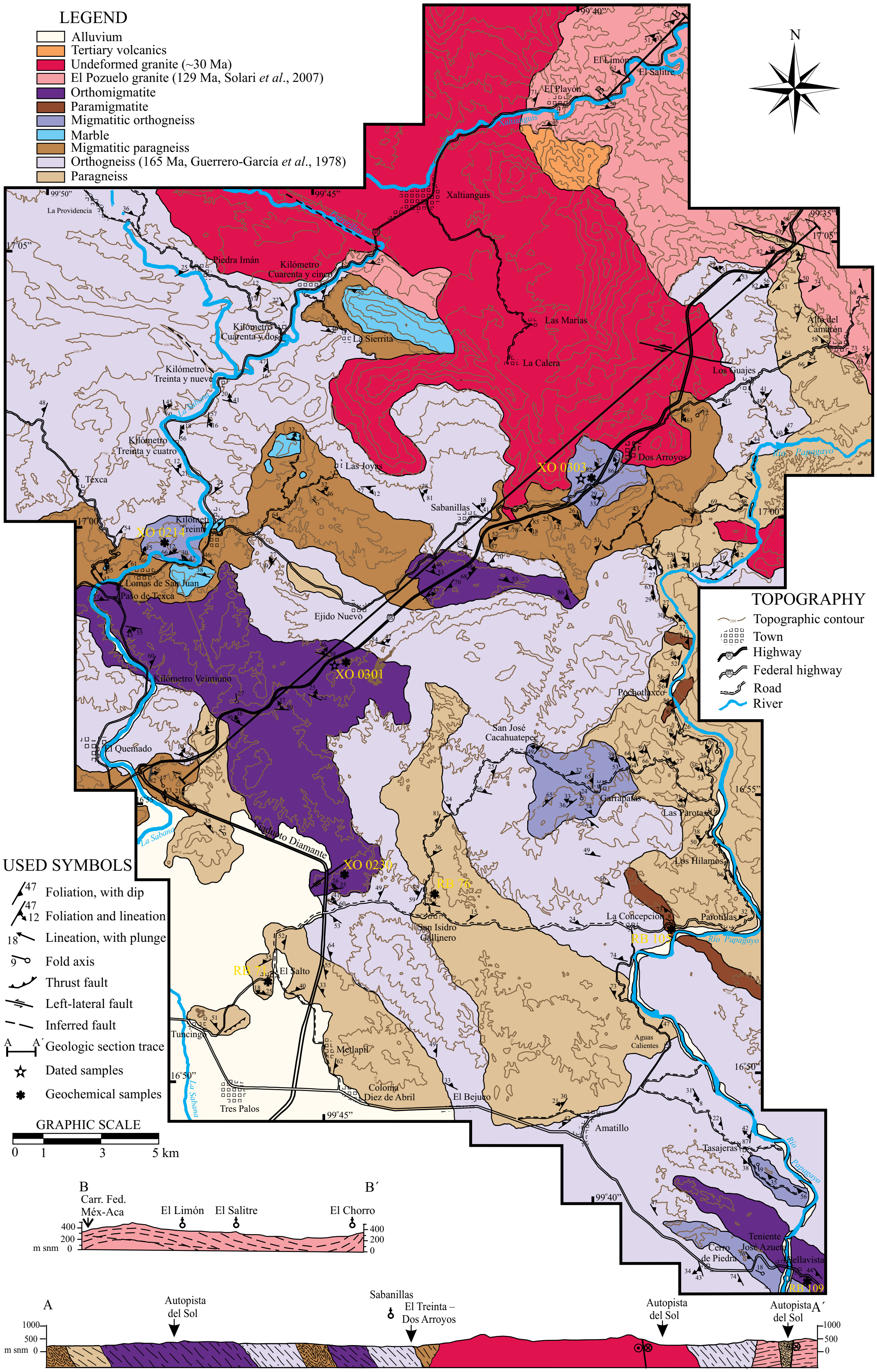

LEGEND
Alluvium
Tertiary volcanics
Undeformed granite (~30 Ma)
El Pozuelo granite (129 Ma, Solari et al., 2007)
Orthomigmatite
Paramigmatite
Migmatitic orthogneiss
Marble
Migmatitic paragneiss
Orthogneiss (165 Ma, Guerrero-García et al., 1978)
Paragneiss
N
TOPOGRAPHY
Topographic contour
Town
Highway
Federal highway
Road
River
USED SYMBOLS
Foliation, with dip
Foliation and lineation
Lineation, with plunge
Fold axis
Thrust fault
Left-lateral fault
Inferred fault
Geologic section trace
Dated samples
Geochemical samples
GRAPHIC SCALE
0 1 3 5 km
99°50"
99°45"
99°40"
99°35"
17°05"
17°00"
16°55"
16°50"
El Limón
El Salitre
El Playón
Xaltianguis
La Providencia
Piedra Imán
Kilómetro Cuarenta y cinco
Kilómetro Cuarenta y dos
La Sierrita
Las Marías
La Calera
Los Guajes
Alto del Camarón
Kilómetro Treinta y nueve
Kilómetro Treinta y cuatro
Texca
Las Joyas
Sabanillas
Dos Arroyos
XO 0303
XO 0214
Lomas de San Juan
Paso de Texca
Ejido Nuevo
XO 0301
Kilómetro Veintiuno
El Quemado
Pochotlaxco
San José Cacahuatepec
Garrapatas
Las Parotas
Los Hilamos
La Concepción
Parotillas
RB 107
Río Papagayo
Viaducto Diamante
XO 0230
RB 76
San Isidro Gallinero
RB 71
El Salto
Tuncingo
Metlapil
Colonia Diez de Abril
El Bejuco
Tres Palos
Aguas Calientes
Amatillo
Tasajeras
Teniente José Azueta
Cerro de Piedra
Bellavista
RB 109
B
B´
Carr. Fed. Méx-Aca
El Limón
El Salitre
El Chorro
400
200
0
m snm
A
A´
Autopista del Sol
Sabanillas
El Treinta – Dos Arroyos
1000
500
0
m snm

those in the Guerrero Terrane (Talavera-Mendoza *et al.*, 2007; Centeno-García *et al.*, 2008). These correlations can be interpreted as the prime evidence for the autochthonous nature of the Xolapa terrane.

Corona-Chávez *et al.* (2006) recognized a single high-grade metamorphic event (830–900 °C and 6.3–9.5 kbar) with a clockwise pressure-temperature (P-T) path in the Xolapa Complex of the Puerto Escondido – Puerto Ángel area (Figure 1). Fluids released by the breakdown of biotite and amphibole produced intense migmatization. The vast majority of plutonic rocks of the Xolapa Complex are calc-alkaline granites and granodiorites (Herrmann, 1994). The Tertiary (Paleocene to Oligocene) granites and granodiorites have similar compositions (Morán-Zenteno, 1992; Schaaf *et al.*, 1995; Morán-Zenteno *et al.*, 1996; Morán-Zenteno *et al.*, 1999; Morán-Zenteno *et al.*, 2005).

ROCK TYPES

The study area, located north of Acapulco, covers about 700 km^2. Previous studies in this area were focused on general field descriptions of the northern part of the Xolapa Complex in the Barranca de Xolapa (Figure 2), where the Xolapa Complex was first defined (De Cserna, 1965). Subsequently, Alaniz-Álvarez and Ortega-Gutiérrez (1997) described medium to high-grade metasediments at this locality (quartz-K-feldspar-biotite-muscovite-sillimanite-garnet, and rare cordierite and corundum) that are intruded by different generations of variably deformed pegmatite, mafic dikes and granites. Other studies dealt with regional geological mapping (*e.g.*, Sabanero-Sosa, 1990), or combined geologic mapping with isotopic determinations (Morán-Zenteno, 1992). For instance Morán-Zenteno (1992) produced a regional map, and geochemical, Rb-Sr and Sm-Nd data on the deformed granitoids, which yielded an age of ~130 Ma, interpreted as the age of intrusion. Other studies north of Acapulco provided geochronological data on gneisses (~134–140 Ma, Ducea *et al.*, 2004) and undeformed, Oligocene plutons (*e.g.*, Herrmann *et al.*, 1994; Schaaf *et al.*, 1995; Ducea *et al.*, 2004), but the lack of detailed mapping makes it difficult to establish a complete geological record. Northeast of the study area, Torres-de León (2005) and Solari *et al.* (2007) documented the allochthonous nature of the Tierra Colorada area (Figure 1). Torres-de León (2005) and Solari *et al.* (2007) established the structural and magmatic evolution of the Tierra Colorada area as a series of alternating magmatic (~130, ~55, and ~34 Ma) and deformation pulses (>130, ~45, and between 45 and 34 Ma).

Our geologic mapping (Figure 2) revealed the existence of several lithologies exposed north of Acapulco that belong to the Xolapa Complex. The recognized pre-migmatitic rocks were grouped into para- and ortho-gneisses, which are affected by variable degrees of migmatization. Their petrographic characteristics and field relationships are described in the following section.

Metasediments

Metasediments, including psammitic-pelitic paragneisses as well as marbles, are mainly distributed to the south and southeast of the study area and constitute ~30% of the area (Figure 2). They generally consists of 5–30 cm thick bands of grey to ochre-brown colored quartzofeldsphatic micaschists, whose main constituents are granoblastic quartz, plagioclase, biotite, muscovite, cordierite, garnet, ± sillimanite, ± staurolite. Staurolite and muscovite are not present in the migmatitic rocks. The association biotite + sillimanite + cordierite + corundum + hercynite is quite common in the metasedimentary restites. Zircon and apatite are common accessory minerals. Tourmaline is an abundant accessory mineral in some samples. Biotite, muscovite and sillimanite (often present as fibrolite) are generally intergrown, and aligned along foliation planes. The mineralogy suggests a greywacke/minor pelites protolith. Up to 1 km wide marble bodies within the sequence are made up of ≤85% calcite, minor dolomite, and accessory quartz, plagioclase, diopside and detrital zircons.

Orthogneisses

Orthogneisses, the most abundant lithology in the study area, are mainly leucocratic to mesocratic, pervasively foliated granites and granodiorites (not distinguished on Figure 2). The orthogneisses are banded and often characterized by up to 20 cm thick dark bands mainly composed of biotite, hornblende, plagioclase and opaque minerals. Leucocratic bands are composed of quartz, plagioclase, potassic feldspar, biotite, ± hornblende. Common accessory minerals are zircon and apatite. Chlorite develops as a secondary mineral phase at the expense of biotite. Orthoclase porphyroclasts are present, sometimes developing core and mantle textures, with sodium-rich mantles around potassium-rich cores. The foliation is defined by biotite and feldspar porphyroclasts in the leucocratic bands, and hornblende and biotite in the melanosomes (*e.g.*, Figure 3a). The sharp contacts between paragneisses and orthogneisses, as well as some preserved cross-cutting relationships, indicate of original intrusive relationships.

Figure 2. Geologic map of the Xolapa Complex between Acapulco and Tierra Colorada, Guerrero, southern Mexico. Modified from Pérez-Gutiérrez (2005).

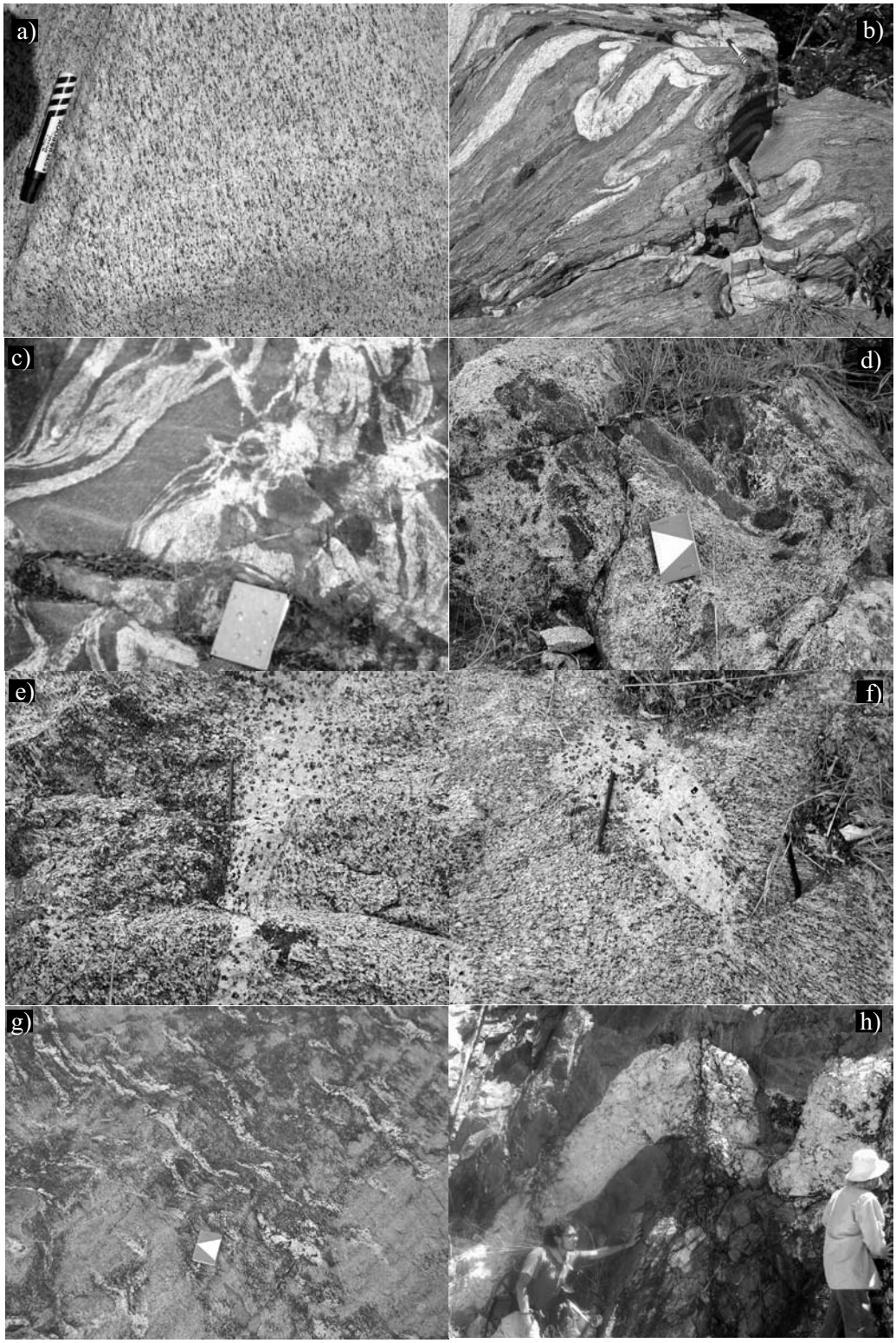

Figure 3. Field photographs illustrating the main aspects of the migmatites cropping out in the studied area. a: Medium-grained orthogneiss, showing S_2 foliation made up of aligned biotite and hornblende: the black marker is ~12 cm long. b: Close to isoclinally folded stromatic migmatite: the black marker on the top center is ~12 cm long. c: Pinch and swell, to agmatic migmatite, with injecting leucosomatic vein, lacking a preferred orientation of intrusion; the notebook is ~16×20 cm in size. d: Raft (Schöllen) migmatite, where dm-sized block of melanosome float into a heterogeneous leucosome; the notebook is ~12×17 cm in size. e: Diktyonitic migmatite, with a vein of leucosome that is intruding the granitic mesosome, showing diffuse contacts; vertical pencil, in the mid of the picture, is ~15 cm long. f: Orthogneiss with granitic leucosome pods, with diffuse contacts, is characterized by centimetric crystals of biotite and hornblende: the pencil is ~15 cm long. g: Leucosome veins, or lens, are intruding the paleosome parallel to S_1 surfaces, but they are not deformed themselves; the notebook is ~12×17 cm in size. h: *ca.* 1 m-thick muscovite and garnet-bearing, F_5 folded pegmatite. Fold axis is roughly subhorizontal and EW oriented. Axial plane is NNE-steeply plunging, ESE-WNW trending.

Ortho- and para-migmatites

Migmatization is superimposed on both ortho- and para-gneisses (Figure 2). The main recognizable types are (following Mehnert, 1968, and modifications in Milord and Sawyer, 2003, and Brown, 2004): (1) stromatic, *i.e.* banded migmatites, where up to 10 cm thick melanosomatic bands, made up of hornblende, biotite, plagioclase, and opaque minerals, alternate with leucosomes made up of quartz, plagioclase, ± feldspar, ± garnet, ± muscovite (Figure 3b); (2) Agmatic to diktyonitic migmatites, in which a breccia-like paleosome is injected by a network of neosome veins (Figure 3c) of trondhjeimitic to tonalitic compositions (the latter often shows green poikiloblasts of hornblende, ± garnet ± biotite); (3) Raft migmatites (Figure 3d), in which small pieces of paleosomatic gneisses float in a heterogeneous leucosome; (4) nebulitic migmatites (Figure 3e), in which the advanced degree of migmatization almost completely erases the original structures of the former gneisses. Pods of granitic leucosome are common, and they generally show centimetric porphyroblasts of biotite and hornblende (Figures 3e and 3f). Based on the degree of migmatization, four different units were mapped (Figure 2): (1) migmatitic paragneisses, *i.e.* rocks with well-preserved gneissosity, <30% of partial melting, and sedimentary (peraluminous) protolith; (2) migmatitic orthogneiss, same as (1) but with igneous protolith; (3) para-migmatite, where the leucosomes constitute >30% and the rock lack of clear, traceable gneiss bands; the abundant Al-rich phases, such as sillimanite and garnet, are indicative of a sedimentary origin; and (4) ortho-migmatite, same as (3), but with a clear igneous protolith suggested by the absence of Al-rich phases, together with the presence of biotite and hornblende as principal mafic phases.

Post-migmatization units

Three groups of post-migmatization rock types were recognized in the study area (Figure 2).

Deformed plutons

The deformed plutons have compositions ranging from granite to granodiorite and locally tonalite. Plutonic rocks cropping out towards the SE of the study area usually display a magmatic foliation that was later overprinted by solid-state deformation (*e.g.*, Morán-Zenteno, 1992). Based on field relations and geochronologic data, Morán-Zenteno (1992) argued that the emplacement of deformed granites was syntectonic with the main tectonothermal event that affected the protoliths of the Xolapa Complex. However, in the N-NNW-vergent, La Venta shear zone, the 129 Ma El Pozuelo granite (Figure 2) was deformed under greenschist facies conditions at ~45 Ma (Torres-de León, 2005; Solari *et al.*, 2007). As the El Pozuelo granite is not sheared outside the ~100 m wide La Venta shear zone, Solari *et al.* (2007) argued that the crystallization of El Pozuelo granite postdates migmatization in the Xolapa Complex. Ducea *et al.* (2004, 2006) also reported ~134 to ~140 Ma U-Pb zircon ages on "syntectonic" hornblende-biotite gneisses in the study area.

Undeformed, post-Laramide plutons

A second group of post-migmatitic granites typically have ~55 Ma ages. They slightly postdate Laramide deformation in southern Mexico (Cerca *et al.*, 2007; Solari *et al.*, 2007). Such bodies lack of solid-state deformation, although they are locally affected by low-grade ductile shearing or brittle deformation. For instance, the Acapulco granite, intruding the Xolapa migmatites and gneisses just SW of the mapped area, was dated by Ducea *et al.* (2004) at 54.9 ± 2 Ma. The Salitre peraluminous and Las Piñas granites were dated at 55.3 ± 3.3 and 54.2 ± 5.8 Ma, respectively (Solari *et al.*, 2007), and crop out northeast of the study area, just west of the La Venta shear zone. The plutons are either foliated (El Salitre) or unfoliated (Las Piñas), and locally, along La Venta shear zone, they display S-C fabrics associated with the shearing.

Eocene-Oligocene undeformed granitoids

A third group of undeformed, Eocene-Oligocene granitoids crop out in the studied area (Herrmann *et al.*, 1994; Schaaf *et al.*, 1995; Ducea *et al.*, 2004; Hernández-Pineda, 2006). These plutonic bodies lack ductile, solid-state deformation, but they generally show magmatic banding as well as brittle faults and joints.

Several generations of dioritic-quartzodioritic dikes, pegmatites, and minor aplites, intrude both the Xolapa basement, and the Eocene-Oligocene granitoids. Some pegmatites cropping out in the Barranca de Xolapa were dated by Morán-Zenteno (1992) at ~59 Ma, and by Solé (2004) at 60–62 Ma. Although no isotopic ages are available for the dioritic dikes, the youngest generation post-dates the 34 Ma Tierra Colorada granite.

STRUCTURAL EVOLUTION

Three phases of ductile deformation were recognized in the gneisses and migmatites of the study area that are absent in the post-migmatization granitoids. Post-migmatization deformation was previously described by Solari *et al.* (2007) as ~45 Ma greenschist facies extension, 45–34 Ma brittle-semibrittle SW-vergent thrusting and open folding.

D_1: metamorphic banding and initial stages of migmatization

S_1 metamorphic banding consists of alternating leucocratic and melanocratic horizons, which range from 0.5 to 10 cm in the orthogneisses but are as thin as few millimeters in paragneisses. Penetrative ductile deformation is associated with development of a gently to moderately,

NE to ENE dipping S_1 foliation in the west and southwest of the study area, whereas it is moderately W to WNW dipping in the east (stereonets of Figures 4a and 4b). Pre-D_1 granitic dikes intruding the paragneisses (*e.g.*, Figure 3c) were deformed by recumbent to isoclinal, rarely rootless, F_1 folds, with axial planes subparallel to the S_1 foliation. S_1 is defined by polygonal quartz, micas and sillimanite in the paragneisses, and by biotite, hornblende and quartz in orthogneisses. The grain size of the quartz varies from band to band. Stretched quartz and elongated feldspar porphyroclasts define the gently NE- to NW-plunging L_1 lineation (Figures 4a and 4b).

D_2/M_2: ductile deformation, migmatization and leucosome emplacement

In the para-gneisses outside the migmatitic zone, a foliation, S_2, is made up of aligned sillimanite + biotite ± muscovite ± staurolite. Garnet is often present in the foliation planes. In the orthogneisses, aligned brown hornblende + biotite + titanite ± garnet constitute S_2 (*e.g.*, Figure 3a). S_1 and S_2 appear to form a composite foliation, $S_{1/2}$, formed at the highest metamorphic grade as part of one continuous tectonothermal event. Undeformed, 1 to 7 cm thick leucosomatic lenses injected into the paleosome parallel to S_1 (Figure 3g) have randomly oriented miner-

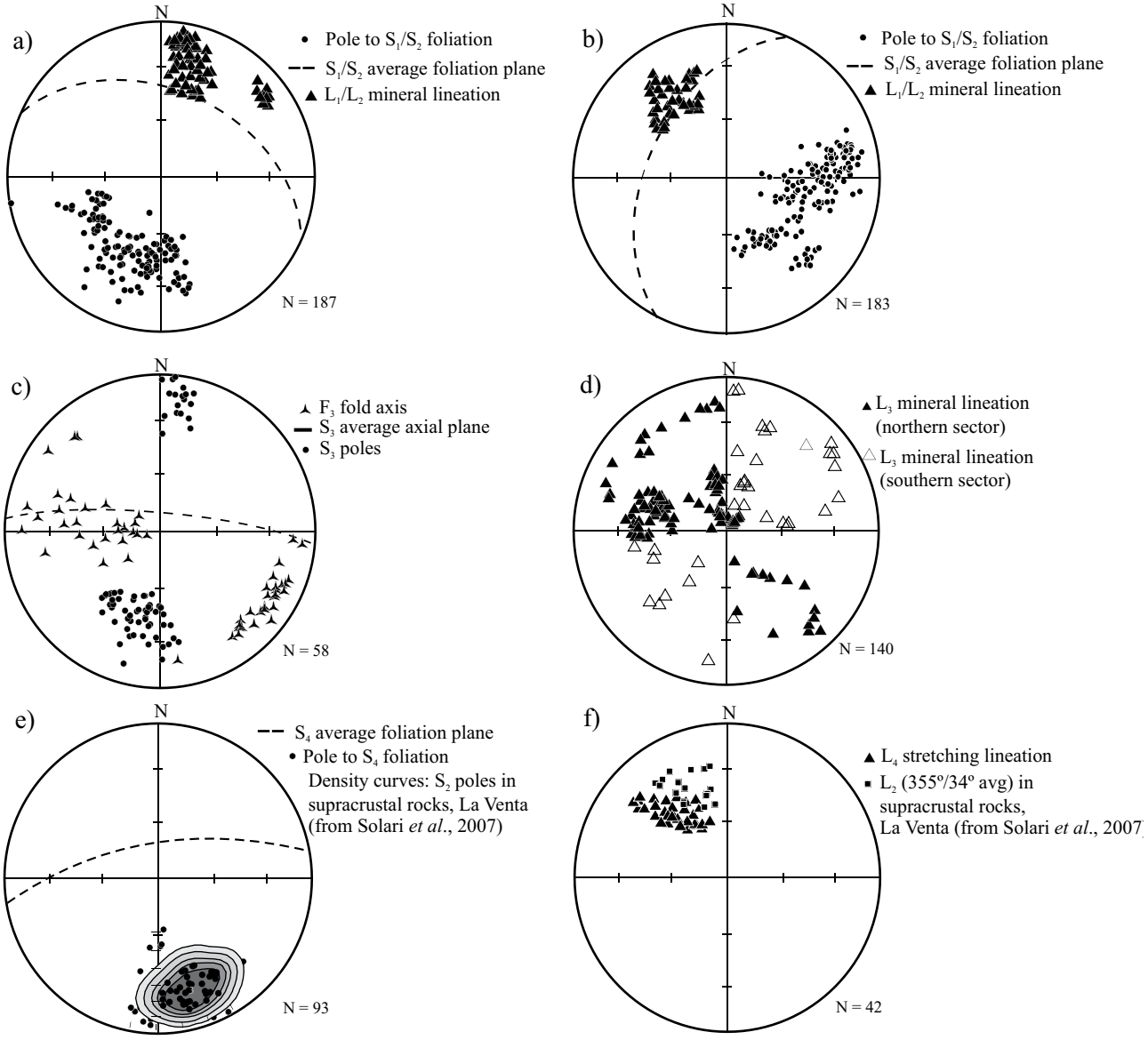

Figure 4. Lower hemisphere stereoplots of structural measured fabrics. a: poles to S_1/S_2 foliation and L_1/L_2 mineral lineation in the western part of the study area. b: poles to S_1/S_2 foliation and L_1/L_2 mineral lineation in the eastern part of the study area. c: F_3 fold axes and the average S_3 axial plane. d: Dispersed L_3 mineral lineation. e: Pole to S_4 foliations measured in the Xolapa Complex. Density curves are an average plot of poles to foliation for the same phase of deformation in the supracrustal rocks of the La Venta area (Solari *et al.*, 2007). f: L_4 stretching mineral lineations. Kinematics, as observed in supracrustal rocks, is normal with a top-to-the NNW component (*cf.* Solari *et al.*, 2007). Squares indicate the average stretching lineation of the same phase of deformation in the supracrustal rocks of the La Venta area (Solari *et al.*, 2007).

als suggesting that the migmatization postdates the D_1 deformation. However, it is possible that the heat associated with D_1 friction was responsible for partial melting, and acted as the driving mechanism for neosome generation during the high-grade metamorphism (*cf.* Brown, 2005). The absence of a S_2 foliation in the migmatites and migmatitic gneisses is inferred to be due to the high ductility of molten leucosome during D_2, which precluded the recrystallizing minerals from becoming oriented (*e.g.*, Solari *et al.*, 2003).

D_3: ductile deformation of migmatitic structures

The $S_{1/2}$ foliation and banding are locally deformed by chevron, gently to moderately NW to SE plunging, subvertical to steeply NNE dipping, slightly asymmetric F_3 folds (Figures 4c and 5a). These folds are common in both the paragneisses and migmatitic gneisses, but are less common in orthogneisses. In paragneisses, the S_3 axial planes are characterized by alignment of biotite and muscovite; in the orthogneisses S_3 is defined by aligned hornblende and biotite (Figure 5b). This suggests that the

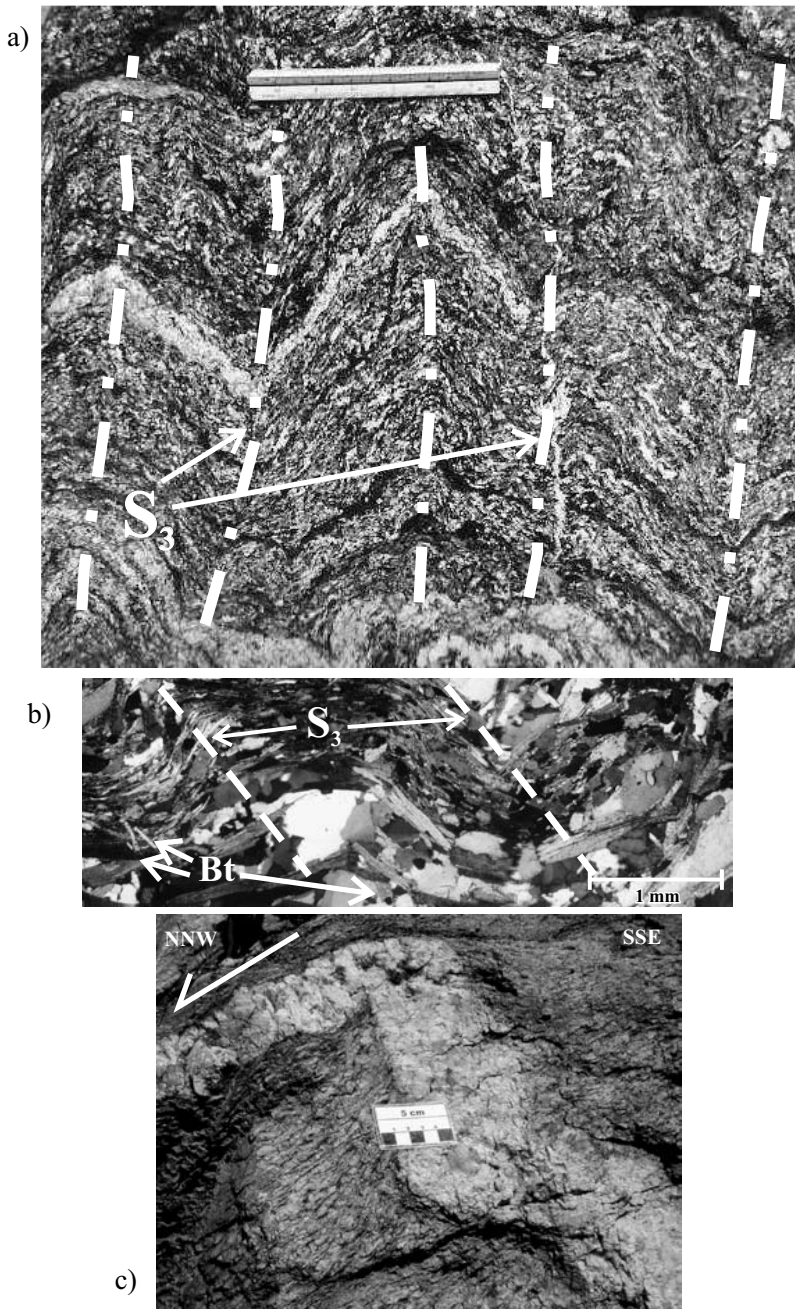

Figure 5. Field and microstructural character of post-migmatitic structures in the Xolapa Complex. a: Mesoscale, chevron F_3 folds; the ruler is 30 cm long. b: microscopic detail of F_3 chevron folds cut perpendicular to the fold hinges: biotite crystals grow parallel to the S_3 axial planes. c: Deflection of the uppermost limb of a S_3 fold by top-to-the NNW-vergent S_4 shear planes; 5 cm scale.

metamorphic grade associated with D_3 was in the upper greenschist to amphibolite facies. A L_3 mineral lineation varies in orientation from north to south in the study area (Figure 4d). This variation is probably due to the later D_4 shearing and D_5 refolding.

D_4: greenschist facies extension in the post-migmatization units

Top-to-the NNW D_4 shear zones, developed under greenschist facies conditions, affected both Xolapa Complex and post-Xolapa Complex units in the northeastern part of the study area (Figure 2). For example, F_3 fold limbs are deflected in the shear zones (*e.g.*, Figure 5c). Whereas S_4 shear zones are mappable in supracrustal rocks of the Chapolapa Formation, and in both post-migmatization ~130 and ~55 Ma granites (*cf.* Solari *et al.*, 2007), in the Xolapa gneisses, S_4 is generally parallel to S_2, constituting a composite S_2/S_4 foliation, associated with a composite $L_{2/4}$ stretching lineation (Figures 4e and 4f, respectively).

D5: folding of ~55 Ma pegmatites

Garnet and muscovite-bearing pegmatites, up to 60 cm thick, were closely folded during D5. The S_5 axial planar cleavage is not present in folded pegmatites, but it is visible in the host paragneisses. F_5 fold axes (*e.g.*, Figure 3h) are roughly subhorizontal, and EW trending, whereas axial plane are subvertical to NNW steeply plunging, and ESE-WNW trending.

SUMMARY OF STRUCTURAL EVENTS IN THE XOLAPA COMPLEX AND ITS COVER

Five phases of ductile deformation have been recognized in the Tierra Colorada area of the Xolapa Complex:

(a) D_1 and D_2 are associated with high-grade metamorphism and migmatization;

(b) D_3 is characterized by chevron folds;

(c) D_4 is present in the northwestern part of the study area, where it is congruent with the ~45 Ma, normal to left-lateral ductile shearing in the La Venta shear zone (D_2 of Solari *et al.*, 2007);

(d) D_5 produced folds in some pegmatites cropping out in the northwestern portion, and it can be correlated with the adjacent SSW-vergent thrusting of the Morelos Fm. over the Chapolapa Fm. (D_3 of Solari *et al.*, 2007).

ANALYTICAL METHODS

Geochemical analyses were performed at Actlabs Labortories (Texas, EE.UU). Major elements were determined by Instrumental Neutron Activation (INA), whereas trace elements were measured by Inductively Coupled Plasma–Mass Spectrometry (ICP-MS) employing lithium metaborate/tetraborate fusions. Common Pb analyses were performed at Laboratorio Universitario de Geoquímica Isotópica, UNAM on feldspars separated from the crushed rocks using methods described in Solari *et al.* (2004).

Zircons were separated by means of standard crushing and concentration techniques, such as Wilfley shaking table, Frantz isodynamic magnetic separator, and heavy liquids (*e.g.*, Solari *et al.*, 2007). About 10 kg of sample were processed to ensure that every morphological type of zircon was adequately represented in the final concentrate. Representative zircons were then handpicked in ethanol, mounted in epoxy resin together with chips of standard zircon R33 (Black *et al.*, 2004). The mount was then ground to expose zircons to approximately half their thickness, and polished using diamond compound. Polished mounts were cleaned in 1N HCl, to avoid surficial common Pb contamination, and gold coated. Cathodoluminescence imaging (CL) was performed on the polished zircons to gain knowledge on their internal morphology, guide the analysis and help later with the age interpretations. CL imaging was performed in a JEOL 5600 LV SEM, equipped with a Hamamatsu CL Detector, in Stanford-USGS facility. A total of 36 analyses, 20 on zircons belonging to sample Xo0301, and 16 on zircons belonging to sample Xo0303 were performed for U-Th-Pb geochronology, following the methodology reported in Nourse *et al.* (2005) and Weber *et al.*, (2006), and utilizing the Stanford-USGS SHRIMP-RG (Sensitive High Resolution Ion Microprobe – Reverse Geometry) facilities. Oxygen was used as primary ion beam, and operated at about 2–4 nA, excavating an area of about 25–30 μm in diameter to a depth of about 1 μm. Sensitivity ranged from 5 to 30 cps per ppm Pb. Data for each spot were collected in sets of five scans through the mass range. Isotope ratios were corrected for common Pb using the measured ^{204}Pb. The reduced $^{206}Pb/^{238}U$ ratios were normalized to the zircon standard R33 which has a concordant TIMS age of 418.9 ± 0.4 Ma (2σ) (Black *et al.*, 2004). For the closest control of Pb/U ratios, one standard analysis was performed after every four unknown samples. Uranium concentrations were monitored by analyzing a standard (CZ3) with ~550 ppm U. U and Pb concentrations are accurate to about 10–20%. SHRIMP isotopic data were reduced using SQUID (Ludwig, 2001) and plotted using IsoplotEx (Ludwig, 2004).

GEOCHEMISTRY

After extensive petrographic screening to eliminate altered samples, six orthogneiss and two paragneiss were chosen for geochemical analysis (Table 1). These samples include unmigmatized samples (RB71 and RB76), gneisses (Xo0303, Xo0230, Xo0214), and migmatites (Xo0301, RB105, RB109). As most of the analyzed samples are high-grade metamorphic rocks, classification and interpretation using diagrams designed for unmetamorphosed rocks should be viewed with caution. Nevertheless, comparisons between

Table 1. Geochemical analyses, Xolapa Complex, Acapulco Tierra Colorada sector, southern Mexico.

Sample #	**RB 71**	**RB 76**	**RB 105**	**RB 109**	**XO 0301**	**XO 0303**	**XO 0230**	**XO 0214**
Rock description	Paragneiss	Orthogneiss	Migmatite Orthogneiss	Migmatite Paragneiss	Migmatite Orthogneiss	Migmatitic Orthogneiss	Migmatitic Orthogneiss	Migmatitic Orthogneiss
Main minerals	Qz-Pl-Bt-Gnt Sil-Op	Pl-Hbl-Qz-Ttn	Qz-Pl-Bt-Gnt	Pl-Bt-Hbl-Gnt-Qz	Qz-Pl-Bt-Hbl-Gnt-Op	Qz-Pl-Bt-Kfs-Gnt-Op	Qz-Pl-Bt-Gnt-Op	Qz-Pl-Bt-Gnt-Op
Lat	N16˚52´23"	N16˚54´07"	N16˚52´37"	N16˚46´32"	N16˚57´29"	N17˚00´56"	N 16°53'36"	N 16°59'22.1"
Long	W99˚46´31"	W99˚43´25"	W99˚52´35"	W99˚36'19"	W99˚44'51"	W99°39'31"	W 99°44'54"	W 99°47'45.5"
SiO_2	70.59	58.78	74.73	68.50	69.32	67.79	69.80	66.25
Al_2O_3	15.21	15.69	13.80	15.68	15.23	15.45	14.69	15.41
Fe_2O_3	2.49	8.00	1.60	3.74	4.22	3.97	4.18	3.63
MnO	0.033	0.116	0.034	0.074	0.073	0.047	0.075	0.050
MgO	0.61	3.60	0.24	0.93	0.80	1.35	0.96	0.77
CaO	2.87	8.91	1.82	4.22	4.41	2.90	3.64	2.01
Na_2O	3.74	2.24	3.85	3.58	3.61	3.58	3.89	3.49
K_2O	2.99	0.91	3.25	2.15	1.28	3.00	1.83	5.22
TiO_2	0.294	0.787	0.141	0.356	0.391	0.640	0.437	0.558
P_2O_5	0.07	0.12	0.04	0.08	0.09	0.14	0.09	0.14
LOI	0.81	0.64	0.51	0.51	0.51	1.13	0.29	1.52
TOTAL	99.69	99.78	100.01	99.81	99.93	99.99	99.87	99.05
Sc	7	29	4	10	12	9	12	8
Zr	125	180	86	134	268	180	168	295
Be	2	1	2	2	2	3	2	1
V	34	190	9	55	47	75	49	26
Cr	-20	38	-20	-20	-20	30	-20	-20
Co	2	16	-1	3	5	4	5	4
Cu	-10	-10	-10	-10	20	11	-10	11
Zn	31	50	-30	38	33	43	77	41
Ga	16	15	15	15	17	17	17	16
Ge	0.8	1.8	0.9	0.8	1.4	0.7	1.2	0.9
Rb	83	12	89	52	52	85	88	108
Sr	181	312	98	290	215	201	171	198
Y	16.0	34.2	30.2	13.1	36.7	27.1	30.5	21.6
Zr	116	176	94	119	264	185	177	287
Nb	4.6	5.9	5.3	4.1	6.3	10.3	7.1	8.6
Sn	3	2	1	-1	2	2	2	1
Cs	2.9	0.2	2.4	1.9	1.4	3.5	2.6	0.9
Ba	667	147	884	1,120	448	1,240	506	2127
La	17.1	16.7	23.1	26.0	27.7	29.5	27.2	50.5
Ce	32.3	35.8	45.6	42.7	57.5	59.0	53.6	100
Pr	3.75	4.48	5.17	4.39	7.19	6.79	5.44	10.3
Nd	13.9	18.6	19.9	15.4	29.1	26.4	21.1	40.2
Sm	2.75	4.56	4.53	2.63	6.39	5.49	4.64	6.77
Eu	0.889	1.03	0.654	0.982	1.46	1.46	0.952	1.31
Gd	2.33	4.95	4.54	2.28	6.29	4.99	4.80	5.97
Tb	0.41	0.93	0.81	0.36	1.10	0.84	0.83	0.78
Dy	2.41	5.33	4.69	2.02	6.80	4.51	4.96	3.99
Ho	0.49	1.07	0.95	0.41	1.38	0.87	0.99	0.76
Er	1.61	3.18	2.87	1.23	4.04	2.61	3.05	2.28
Tm	0.263	0.512	0.438	0.202	0.569	0.382	0.465	0.339
Yb	1.75	3.31	2.85	1.40	3.50	2.45	2.99	2.27
Lu	0.279	0.490	0.428	0.233	0.515	0.380	0.445	0.341
Hf	3.5	5.1	3.3	3.3	7.3	5.0	4.4	6.8
Ta	0.40	0.45	0.39	0.30	0.40	0.68	0.39	0.61
W	-0.5	1.8	-0.5	-0.5	-0.5	0.6	-0.5	-0.5
Tl	0.85	0.14	0.76	0.55	0.29	0.93	0.65	0.81
Pb	10	8	15	8	7	23	9	17
Bi	2.1	1.6	0.5	0.2	1.0	1.2	0.2	0.2
Th	6.67	6.92	9.77	8.10	6.67	9.75	9.10	12.0
U	1.89	2.57	1.87	1.63	1.74	1.81	1.96	1.38
$^{206}Pb/^{204}Pb^{\dagger}$	N.D.	N.D.	19.00897	19.29560	19.1791	18.91633	19.0978	18.7343
$^{207}Pb/^{204}Pb^{\dagger}$	N.D.	N.D.	15.67733	15.68175	15.6874	15.66799	15.6826	15.6554
$^{208}Pb/^{204}Pb^{\dagger}$	N.D.	N.D.	38.81786	38.85647	38.9359	38.83747	38.8639	38.7383

Major element concentration in wt. %; trace element concentrations in parts per million, determined by ICP-MS at ACTLABS laboratories. Negative numbers are below the detection limit. †: Feldspar measured initial ratios, following Solari *et al.* (2004). 2-sigma errors on isotopic ratios are <0.06% ($^{206}Pb/^{204}Pb$ ratios), <0.08% ($^{207}Pb/^{204}Pb$ ratios) and <0.1% ($^{208}Pb/^{204}Pb$ ratios), respectively.

the compositions of the analyzed samples and pristine igneous rocks can provide some useful insights into the sources and processes that lead to their formation.

The rocks can be classified as metaluminous I-type diorites to granites, displaying a variable range in SiO_2 (58.8 to 74.7 wt%) that correlates negatively with TiO_2, MgO and Fe_2O_3 contents. On the AFM diagram, the rocks plot in the calc-alkaline field (Figure 6a). MgO contents (3.6–0.2 wt%) and Mg# (51–26) of the studied rocks indicate that they are significantly more differentiated than any magma in equilibrium with the upper mantle (Langmuir and Hanson, 1980), and therefore cannot be considered as primary mantle melts.

Chondrite-normalized rare earth patterns (Figure 6e) are enriched in light-rare earth elements (LREE; La/Sm_N 2.3–6.2), and unfractionated in the heavy rare earths (HREE;

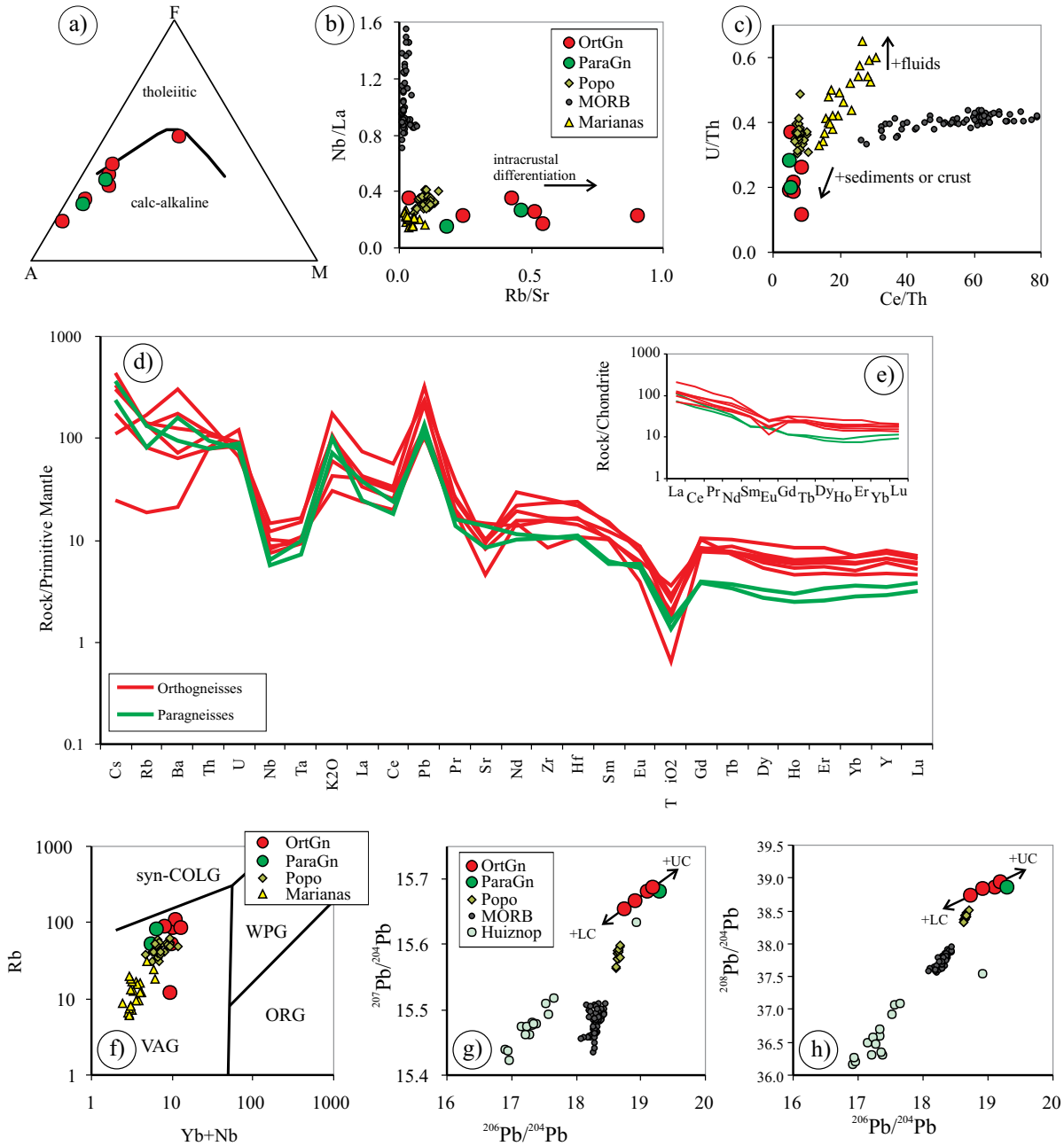

Figure 6. Geochemical data for migmatites and gneisses of the Xolapa Complex plotted in diagrams. a: AFM diagram; b: Rb/Sr *vs.* La/Nb diagram; c: Ce/Th *vs.* U/Th diagram; d: Trace element geochemical composition of selected samples, normalized to the primitive mantle values of Sun and McDonough (1989); e: REE elements normalized to the chondrite values of McDonough and Sun (1995); f: Y+Nb *vs.* Rb tectonic discrimination diagram, after Pearce *et al.* (1984). Syn-COLG: syn-collisional granites; VAG: volcanic-arc granites; WPG: within-plate granites; ORG: Ocean-ridge granites. g: Uranogenic $^{206}Pb/^{204}Pb$ *vs.* $^{207}Pb/^{204}Pb$ diagram; h: thorogenic $^{206}Pb/^{204}Pb$ *vs.* $^{208}Pb/^{204}Pb$ diagram. Reference data of MORB analyses reported in Figures b, c, f and g are from Lehnert *et al.* (2000). Geochemical data of the Mariana arc in Figures b and c are from Elliott *et al.* (1997). Popocatépetl volcano geochemical data (Popo in Figures b, c, f, and g) are from Schaaf *et al.* (2005). Huiznopala gneiss isotopic data (Huizno in Figures f and g) from Lawlor *et al.* (1999).

Dy/Yb_n 1.0–1.4). The Xolapa orthogneisses also display strong negative Eu anomalies (Eu/Eu*=0.44–1) that are coupled with high Rb/Sr ratios (Figure 6b). These geochemical features indicate that magmatic differentiation occurred in the stability field of plagioclase.

Incompatible trace element patterns show enrichments of large ion lithophile elements (LILE) over high-field strength elements (HFSE) typical of arc magmas (Figure 6d). The rocks also display low Nb/La ratios (Figure 6b) and incompatible element relationships that invariably plot within the field of volcanic-arc granites in the tectonic discrimination diagrams of Pearce *et al.* (1984) (Figure 6f). Nonetheless, the Xolapa rocks also tend to have much lower U/Th and Ce/Th ratios (Figure 6c) than is typical for oceanic island arcs, which tend to preserve the chemical signature of fluids released from the downgoing slab. Thus, the relative enrichment in the fluid-immobile element Th likely indicates strong continental contributions to the original magmas, either through subducted sediments or by means of crustal contamination.

Crustal contributions are also supported by the overall radiogenic Pb isotopic compositions of feldspars from the orthogneisses, which form a restricted positive correlation that is bracketed between an evolved upper-crustal-like component similar to the isotopic composition of the analyzed paragneiss, and an unradiogenic lower-crustal-like component with higher $^{207}Pb/^{204}Pb$ and $^{208}Pb/^{204}Pb$ ratios that is typically observed in magmas derived from the partial fusion of the upper mantle (Figures 6g and 6h). In summary, the chemical compositions of the Xolapa rock suites likely reflect the differentiation stages of a magmatic arc that either grew in close proximity to a continent, or was directly constructed over a mature continental crust.

GEOCHRONOLOGY

Two samples of migmatitic orthogneiss were chosen for SHRIMP-RG U-Pb analysis. Sample Xo0301 is a migmatite leucosome made up of quartz, plagioclase (Ab 30–50%), poikilitic garnet, brown biotite, and rare hornblende porphyroclasts. Large allanite crystals, abundant zircon and apatite are common accessory minerals. Sample Xo0303 is a banded migmatitic gneiss, in which leucocratic portions are made up of quartz, plagioclase and subordinate K-feldspar and zircon, whereas mesocratic bands are almost entirely composed of biotite, magnetite, tiny relict garnet, apatite and subordinate zircons as inclusions within biotite. Samples locations are in Figure 2, whereas samples coordinates can be found in Table 1.

Sample Xo0301: migmatitic leucosome

Zircons from sample Xo0301 are pale yellow to honey-colored, range from 60 μm to >250 μm, and show oscillatory zoning in cathodoluminescence (CL) images (Figures 7a to 7l) , which is generally interpreted as igneous zoning (Connelly, 2001; Corfu *et al.*, 2003). Some of the zircons show the presence of xenocrystic cores, whose structures are discordant with igneous oscillatory zoning, indicating that igneous zircon grew around preexisting, undissolved, older zircons. SHRIMP analyses were focused on the igneous zoning and late-stage recrystallization rather than the inherited cores. Analyses yielded two age groups (Figure 8a): (i) seven analyses (discontinuous ellipses in Figure 8b) are concordant to nearly concordant, and have $^{206}Pb/^{238}U$ ages between 135.5 ± 1.0 and 131.3 ±0.7 Ma (1 sigma); and (ii) five analyses (thick line ellipses in Figure 8b) are concordant within the analytical error, and have $^{206}Pb/^{238}U$ ages between 129.8 ± 1.0 and 126.2 ± 1.3 Ma (1 sigma). Comparing the analyzed spots with the CL images (*e.g.*, Figures 7a to 7l), it is evident that the two age groups are related to different events. Whereas, some of the analyzed zircons show continuous oscillatory zonation with similar ages in both core and rim (*e.g.*, Figures 7b, 7c, and 7e), others show a clear discontinuity between core and rim. In one case (Figure 7d), a 129.5 Ma zircon rim grew over an oscillatory-zoned core with a $^{206}Pb/^{238}U$ age of 135.5 Ma. The Early Cretaceous age group, clustering at 133.6 ± 0.9 Ma (Figure 8b) is interpreted as the age of migmatization. The second age group clustering at 129.2 ± 0.4 Ma, is interpreted as either an episode of Pb loss and/or partial recrystallization.

Another group of analyzed spots yielded more discordant isotope ratios, generally with larger errors (Figure 8a). However, the apparent $^{206}Pb/^{238}U$ ages of such zircons define a mean of 61.4 ± 1.5 Ma (Figure 8c), which is interpreted as Early Paleocene Pb loss or zircon growth. CL imaging of such domains (*e.g.*, Figures 7a, 7h, 7i, 7l) reveal that they cannot be texturally distinguished from the first episode of Pb loss or recrystallization at ~129 Ma.

Sample Xo0303: banded migmatitic orthogneiss

Zircons separated from sample Xo0303 are yellow to reddish colored, <280 μm in size, and range from prismatic to stubby with or without bypyramidal terminations. Imaged under CL, most of them show well-developed oscillatory zoning. Inherited cores are visible in some crystals, but they do not show any significant age difference (*e.g.*, Figure 6m) when compared to the oscillatory overgrowths (*e.g.*, Figures 7n to 7r). The isotopic analyses are concordant within analytical error (Figure 9a and Table 2). Together, they define a cluster yielding an average concordia age of 178.7 ± 1.1 Ma interpreted as the crystallization age of the orthogneiss (Figure 9b). Some zircon crystals have brighter rims around oscillatory zones (*e.g.*, Figures 7s to 7z), and analyses of these rims yielded discordant ages (Figure 9a) with $^{206}Pb/^{238}U$ ages ranging between 168.7 ± 1.2 Ma and 116.2 ± 1.0 Ma, suggesting variable degrees of Pb loss. Two

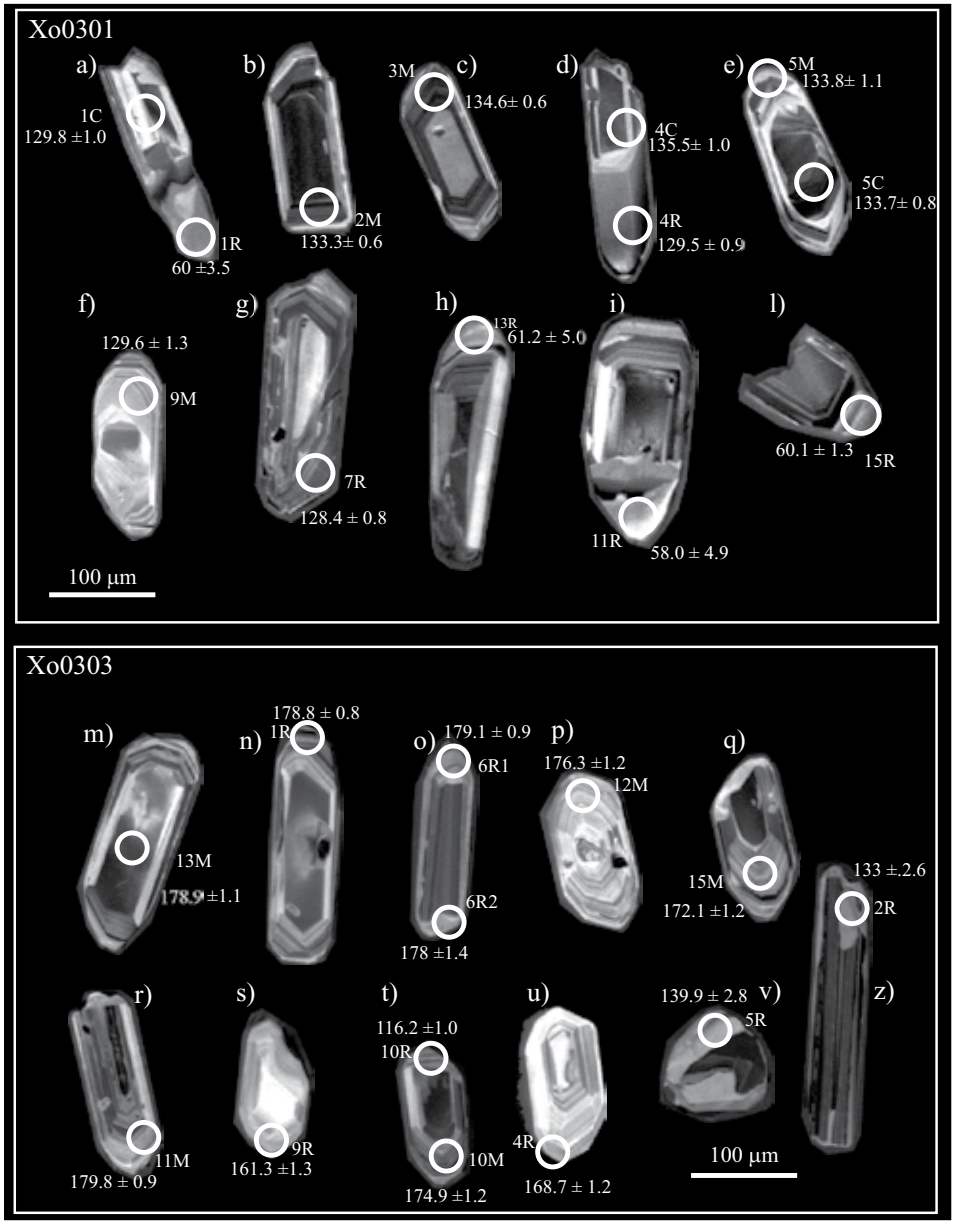

Figure 7. Cathodoluminescence images of selected zircons of the dated samples. a to l: zircons from sample Xo0301. m to z: zircons from sample Xo0303. White bars represent 100 micrometers scale. See text for further explanations.

of the analyzed crystals, although discordant (Figures 7v and 7z, and Table 2), have $^{206}Pb/^{238}U$ ages that are similar to the migmatization age of 133.6 ± 0.9 Ma determined on sample Xo0301. The youngest, discordant analysis (Figure 9a) is probably the result of a younger Pb loss as the youngest zircons analyzed in sample Xo0301.

DISCUSSION AND CONCLUSIONS

Early Jurassic magmatism

The 178 ± 1.1 Ma igneous age calculated from the migmatitic orthogneiss Xo0303 is the first report of a Lower Jurassic magmatic event in the Xolapa Complex (time scale of Gradstein *et al.*, 2004). Because of its calc-alkaline geochemical signature, we argue that the igneous activity is related to a magmatic arc. This is similar to: (a) a Middle Jurassic age of 165 Ma reported by Guerrero-García *et al.* (1978) from the Acapulco – Tierra Colorada transect of the Xolapa Complex; (b) a ~158 Ma age reported by Ducea *et al.* (2004) from north of Puerto Escondido; and (c) an Early Jurassic magmatic age reported by Elías-Herrera *et al.* (2000) in the Tizapa metagranite (186.5 ± 7.4 Ma, lower intercept of discordant data) in the eastern Guerrero Terrane, Teloloapan subterrane, 200 km north of the studied area (Figure 2). The Lower Jurassic age has several paleogeographic implications. First, it indicates the

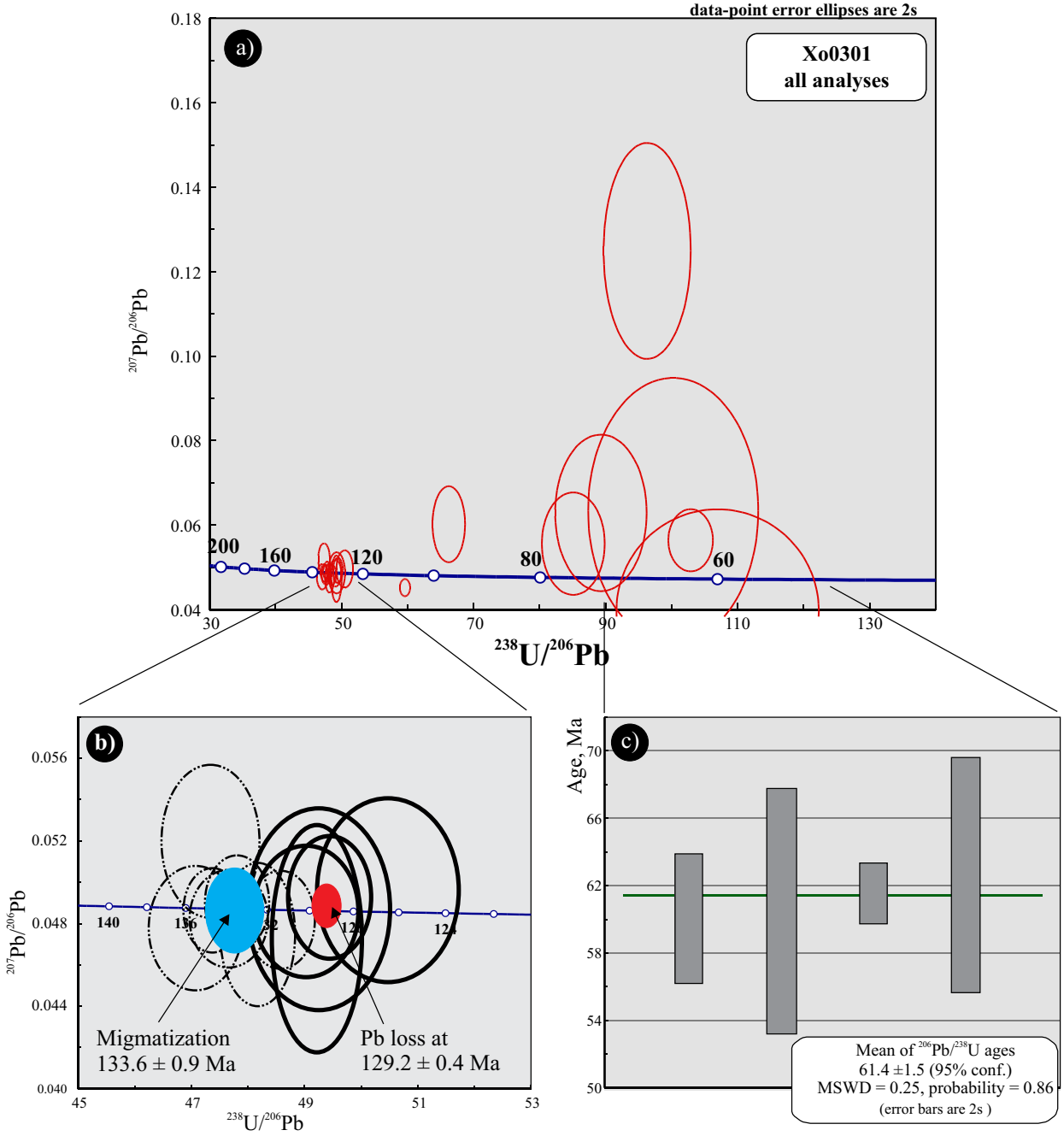

Figure 8. U-Pb concordia plots for sample Xo0301. a: U-Pb Tera-Wasserburg concordia of all the analyses performed on zircons from sample Xo0301; b: Detail of the concordia plot (a) with the interpreted average representing the migmatization and Pb-loss events; c: Mean of $^{206}Pb/^{238}U$ ages for the Early Paleocene overgrowths recognized in some of the analyzed zircons. See text for further explanations.

presence of a pre-Toarcian sedimentary sequence, which was intruded by the Early Jurassic igneous protolith and then metamorphosed to form the Xolapa paragneiss. Ortega-Gutiérrez and Elías-Herrera (2003) argued that ammonite-bearing sediments of the mid-JurassicTecocoyunca Group (Burckhardt, 1927; Corona-Esquivel, 1981), which are extensively exposed north of the Tierra Colorada-Chacalapa shear zone, grade into the metasedimentary protolith of the Xolapa Complex. However, this suggestion is not supported by the data presented in this paper because the Tecocoyunca Group is younger than pre-178 Ma paragneisses of the Xolapa Complex. Another possibility is that the rocks in the study area are correlatives of the easternmost part of the Guerrero Terrane, *i.e.*, the Teloloapan subterrane (Elías-Herrera *et al.*, 2000; Centeno-García *et al.*, 2008). The Teloloapan terrane was accreted to the backbone of Mexico (Mixteca and Zapoteco terranes) either during the Middle-Late Jurassic (Elías-Herrera *et al.*, 2000), during the

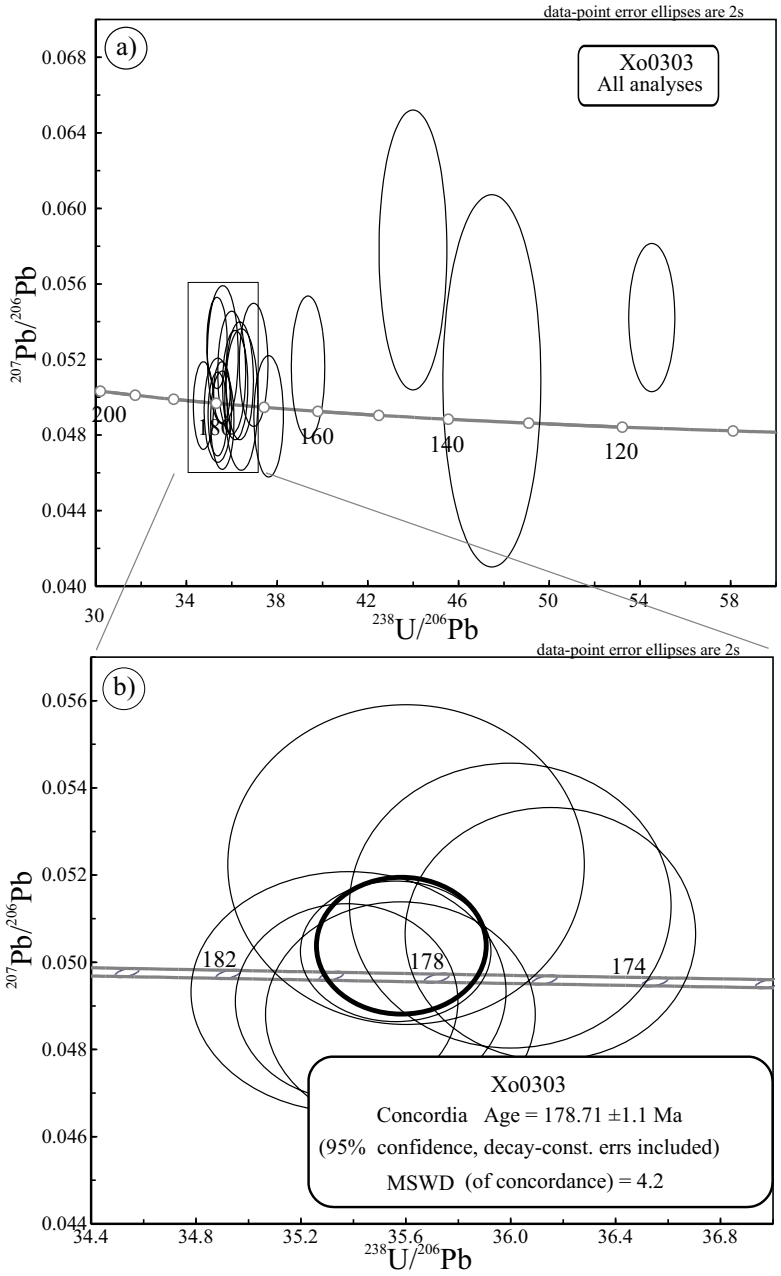

Figure 9. U-Pb concordia plots for sample Xo0303. a: U-Pb Tera-Wasserburg concordia of all the analyses performed on zircons from sample Xo0303; b: Detail of the concordia plot (a) with the interpreted average representing the magmatic age of sample Xo0303. See text for further explanations.

Early Cretaceous (Dickinson and Lawton, 2001), or during the Late Cretaceous (Talavera-Mendoza *et al.*, 2007). Thus, the 178 Ma magmatism in the high-grade Xolapa Complex could have been part of an Early Jurassic magmatic arc fringing the Mixteca Terrane of southern Mexico, which was subsequently accreted and deformed.

Early Cretaceous Migmatization

Our zircon ages indicate that high-grade metamorphism and migmatization of the Xolapa Complex in the study area occurred ~133 Ma ago. This interpretation is consistent with field observations reported by Solari *et al.* (2007), who concluded that migmatization occurred prior tothe ~129 Ma crystallization age of undeformed granites intruding migmatites. Our structural data and petrographic studies of Xolapa high-grade rocks are also consistent with those of Corona-Chávez *et al.* (2006) in the Puerto Escondido area (Figure 1), where only one high-grade metamorphic event in the lower granulite facies is discernible in migmatites and gneisses. Similar lithologies, metamorphic grade and intrusive relationships (*cf.* Robinson *et al.*, 1989; Herrmann *et al.*, 1994; Corona-Chávez *et al.*, 2006) through-

Table 1. U-Pb data table, Xolapa Complex, Acapulco Tierra Colorada sector, southern Mexico.

Grain Spot	$^{206}Pb^{*}$ ppm	U ppm	Th ppm	Th/U	Observed ratios								Apparent ages			
					$^{204}Pb/^{206}Pb$	$^{206}Pb_c$ (%)	$^{207}Pb^{*}/^{206}Pb^{*}$	± 1σ %	$^{208}Pb^{*}/^{206}Pb^{*}$	± 1σ %	$^{206}Pb^{*}/^{238}U$	± 1σ %	$^{206}Pb/^{238}U$ (Ma)	± 1σ	$^{208}Pb/^{232}Th$ (Ma)	± 1σ
	(1)					(2)	(3)		(3)		(3)		(4)		(4)	
Xo0301																
0301-16R	0.5	54	1	0.02	0.03820	9.81	0.12490	8.4	0.19386	11.0	0.00558	2.7	19.2	12.5	---	---
0301-1R	0.1	13	0	0.01	(-)	-0.95	0.03968	24.8	0.08513	31.3	0.01675	8.4	60.0	3.5	---	---
0301-15R	2.2	265	2	0.01	0.00197	1.16	0.05640	5.3	0.03809	9.3	0.01680	4.4	60.1	1.3	---	---
0301-11R	0.1	13	0	0.02	0.00509	2.04	0.06344	20.2	0.10006	21.9	0.01706	5.0	58.0	4.9	---	---
0301-13R	0.4	46	1	0.01	0.00801	1.95	0.06288	12.0	0.07112	16.2	0.00986	4.4	61.2	5.0	---	---
0301-14R	1.4	140	1	0.01	0.00492	1.02	0.05560	8.9	0.04969	13.9	0.00791	3.2	68.5	4.1	---	---
0301-6R	1.6	121	11	0.10	0.00193	1.55	0.06020	6.1	0.07986	7.2	0.00965	1.8	93.2	2.3	---	---
0301-19M	14.0	969	569	0.61	0.00004	-0.38	0.04518	1.9	0.20386	3.0	0.03889	14.8	107.2	0.6	113	4
0301-12M	8.3	486	141	0.30	0.00011	0.13	0.04960	3.6	0.09425	2.6	0.03494	3.8	126.2	1.3	120	5
0301-7R	9.8	561	164	0.30	0.00029	0.08	0.04927	2.5	0.10101	2.3	0.03748	4.7	128.4	0.8	122	8
0301-9M	3.1	180	58	0.33	(-)	0.01	0.04869	4.1	0.10758	3.9	0.03551	3.8	129.6	1.3	132	5
0301-4R	8.4	479	63	0.14	0.00008	-0.17	0.04729	4.8	0.04741	3.7	0.03307	4.7	129.5	0.9	134	8
0301-1C	8.3	474	240	0.52	0.00017	-0.01	0.04859	2.7	0.16726	2.1	0.03145	0.6	129.8	1.0	126	4
0301-8M	14.1	794	269	0.35	0.00004	-0.06	0.04819	2.0	0.11538	1.8	0.03643	3.6	131.3	0.7	135	3
0301-10M	11.2	628	265	0.44	(-)	-0.15	0.04747	3.0	0.13899	1.9	0.03558	3.4	132.4	0.7	133	3
0301-2M	16.5	916	399	0.45	0.00007	0.04	0.04903	1.9	0.14531	1.6	0.03632	4.2	133.3	0.6	133	2
0301-5C	15.3	851	495	0.60	0.00004	-0.06	0.04824	2.0	0.19158	1.5	0.03584	4.3	133.7	0.8	134	2
0301-5M	7.1	391	106	0.28	0.00039	0.41	0.05200	2.9	0.09159	3.1	0.03159	1.9	133.8	1.1	117	11
0301-3M	20.6	1135	818	0.74	0.00004	-0.01	0.04865	1.7	0.23496	1.1	0.03621	3.9	134.6	0.6	133	2
0301-4C	11.0	601	345	0.59	(-)	-0.12	0.04778	2.6	0.18632	1.8	0.03649	2.4	135.5	1.0	134	3
Xo0303																
0303-10R	6.8	429	15	0.04	0.00046	0.74	0.05422	3.0	0.02618	5.9	0.02669	0.9	116.2	1.0	91	76
0303-2R	1.0	56	22	0.42	0.00056	0.27	0.05087	7.9	0.19519	5.2	0.04347	1.7	133.0	2.6	177	17
0303-5R	2.2	111	2	0.02	0.00188	1.12	0.05780	5.2	0.01869	17.3	0.02001	5.8	139.9	2.8	---	---
0303-9R	6.5	298	33	0.11	0.00016	0.29	0.05159	3.0	0.04156	4.4	0.04440	3.2	161.3	1.3	161	20
0303-4R	7.9	347	51	0.15	0.00012	-0.06	0.04899	2.7	0.05071	3.7	0.04634	2.4	168.7	1.2	162	10
0303-15M	7.8	335	140	0.43	(-)	0.28	0.05172	2.6	0.13925	2.2	0.04734	3.4	172.1	1.2	176	4
0303-14M	5.8	248	93	0.39	0.00010	0.04	0.04988	3.1	0.12658	2.8	0.04652	3.5	174.3	1.4	176	6
0303-10M	8.4	357	141	0.41	(-)	0.16	0.05087	2.5	0.13355	3.6	0.04814	3.6	174.9	1.2	181	7
0303-7M	10.0	423	87	0.21	(-)	0.13	0.05064	2.3	0.06672	2.8	0.04710	2.7	175.9	1.1	175	5
0303-12M	8.1	338	108	0.33	0.00007	0.21	0.05131	2.6	0.10748	2.5	0.04644	3.0	176.4	1.2	178	6
0303-6R2	6.9	285	47	0.17	0.00009	0.33	0.05224	2.9	0.05681	3.8	0.04714	2.7	178.3	1.4	176	10
0303-1R	29.8	1232	24	0.02	0.00009	0.08	0.05027	1.3	0.00707	4.9	0.04940	3.7	178.5	0.7	105	42
0303-13M	11.0	455	232	0.53	0.00011	-0.11	0.04879	2.2	0.16618	1.7	0.05097	2.9	178.3	1.1	174	5
0303-6R1	14.6	602	13	0.02	0.00017	0.40	0.05287	1.9	0.01269	5.3	0.05077	3.7	179.3	1.0	150	83
0303-8M	11.0	454	274	0.62	0.00007	-0.04	0.04932	2.3	0.19124	1.7	0.04432	5.8	179.4	1.2	172	4
0303-11M	17.7	728	145	0.21	0.00010	-0.07	0.04911	1.8	0.06716	2.2	0.04875	3.2	179.4	0.9	176	6

(1): Contribution of common ^{206}Pb to total ^{206}Pb in %; (2): Concentration of radiogenic (*) ^{206}Pb; (3): Measured isotope ratios. Errors are provided as 1-sigma in %; (4): Appearent ages, and ^{204}Pb corrections are calculated using SQUID software (Ludwig, 2001). For Phanerozoic zircons in general, $^{206}Pb/^{238}U$ ages, are considered as the most reliable.
- ^{204}Pb not detected; --- $^{208}Pb/^{232}Th$ age and errors were not calculated, because Th is virtually absent in such zircons, and uncertainty is thus too big.

out the Xolapa Complex suggest that the Early Cretaceous age of migmatization can be extrapolated across the whole complex. Support for this is provided by the 131.8 ± 2.2 Ma age calculated by Herrmann *et al.* (1994) on a migmatite cropping out north of Puerto Escondido.

Late Mesozoic to Early Cenozoic evolution

High-grade gneisses and migmatites in the study area underwent limited re-heating during the Late Cretaceous-Paleocene as indicated by Pb loss in zircons of sample Xo0301. Four tectonothermal events were previously reported for the early Cenozoic in the Xolapa Complex: (1) magmatism at ~55 Ma (Acapulco, El Salitre and Las Piñas granites, Morán-Zenteno, 1992; Ducea *et al.*, 2004; Solari *et al.*, 2007); (2) NNW-vergent, normal and left-lateral ductile shearing at ~45 Ma (Riller *et al.*, 1992; Solari *et al.*, 2007); (3) SW-vergent brittle thrusting between ~45 and ~34 Ma, and (4) magmatism at ~30–34 Ma (Tierra Colorada and Xaltianguis undeformed granites, Herrmann *et al.*, 1994; Schaaf *et al.*, 1995; Ducea *et al.*, 2004; Hernández-Pineda, 2006). Such events are probably responsible for the reorientation of previous structures (*e.g.*, D_4, see above), Pb loss in zircons, recrystallization or resetting of isotopic chronometers in micas due to intrusion or hydrothermal fluid circulation, specially along the boundaries of major intrusions (*e.g.*, Solé, 2004).

Tectonic implications

Previous studies of the geological record of the Xolapa Complex have been interpreted in terms of extension and exhumation during the Late Cretaceous – Early Tertiary causing uplift of the isotherms and partial melting (*e.g.*, Robinson *et al.*, 1989; Herrmann *et al.*, 1994; Meschede *et al.*, 1997). Such models were partly based on a 66–46 Ma age for the migmatization (Herrmann *et al.*, 1994). These authors suggested that exhumation of the Xolapa Complex was related to the southeastward displacement of the Chortís block from a location off Puerto Vallarta along the southern Mexican coast at ~100 Ma, towards a location off Huatulco at ~29 Ma.

Our present data suggest two alternative models for the Lower Cretaceous migmatization, both involving accretion of outboard terranes: (1) accretion of the Guerrero terrane to the backbone of southern Mexico could possibly have occurred during the Early Cretaceous (but see discussion above); or (2) accretion of the Chortís block to southern Mexico. The absence of an exposed suture east of the Guerrero terrane argues against hypothesis #1, which suggests that the Guerrero terrane may have been a continental margin arc (*cf.* Elías-Herrera and Ortega-Gutiérrez, 1998). Moreover, the accretion of the Guerrero terrane cannot explain the synchronous migmatization as far as 500 km SE of the study area. Several lines of evidence indicate a possible correlation between the Xolapa Complex and the northern Chortís block: (i) a similar metamorphic grade occurs in the exposed basement of Las Ovejas Complex in southern Guatemala and northwestern Honduras (Horne *et al.*, 1976; Schwartz, 1977; Ortega-Gutiérrez *et al.*, 2007; Martens *et al.*, 2007), (ii) a ~170 Ma magmatic arc is present in the Chortís block (Martens *et al.*, 2007), and (iii) the presence of eclogites in the Motagua mélange (central Guatemala), which have Sm-Nd mineral isochron ages spanning ~125 to ~136 Ma (Brueckner *et al.*, 2005; Martens *et al.*, 2007). These latter ages are interpreted in terms of collision between the Chortís block and southern Mexico (*cf.* Harlow *et al.*, 2004; Martens *et al.*, 2007). The similar ~133 Ma migmatization age in the Xolapa Complex could represent collision between the Xolapa Complex and the (current) northern margin of the Chortís block marked by the HP metamorphism in the Motagua melange. Exhumation of such eclogites in blueschist metamorphic conditions at ~70–75 Ma (*e.g.*, Harlow *et al.*, 2004; Martens *et al.*, 2007) could mark the separation of the Chortís block from southern Mexico. This is consistent with the conclusions of Corona-Chávez *et al.* (2006), who suggested that the clockwise P-T path followed by the Xolapa Complex represent a compressional regime in the roots of a continental magmatic arc. Other processes, such as shortening due to accretion of nappes and/or terranes (*e.g.*, Whitney *et al.*, 1999), or magma-loading processes (*e.g.*, Brown, 1996; Warren and Ellis, 1996) are normally invoked in such a tectonic scenario. Removal of the Chortís block during the mid-Late Cretaceous would have allowed reorganization of plates, and onset of subduction along the Middle America trench to generate the ~55 and ~30 Ma arc plutons that intrude the Xolapa Complex (Ducea *et al.*, 2004; Solari *et al.*, 2007) and the Guerrero terrane (*e.g.*, Levresse *et al.*, 2004).

ACKNOWLEDGEMENTS

Several people are thanked for their support during field work (*e.g.*, Rafael Torres de León, Guillermo Hernández Pineda, Teodoro Hernández Treviño, Bernardo Villacura), and for fruitful discussions on the geology of the Xolapa Complex in various stages of this work, such as Pedro Corona-Chávez, Fernando Ortega-Gutiérrez, Mariano Elías-Herrera, J. Duncan Keppie. The authors acknowledge a CONACyT scholarship to RPG, CONACyT grant 54559 to LAS, and PAPIIT-DGAPA grant IN101407 to LAS, which funded field and analytical work. Diego Aparicio made a lot of thin sections we studied during different stages of this work, and Consuelo Macías helped with mineral separations. We also thank Joe Wooden, USGS at Stanford University, for assistance during SHRIMP analyses. Thorough reviews by Bodo Weber, Pedro Corona-Chávez and Dante Morán-Zenteno improved the readability of the concepts expressed in this work.

REFERENCES

Alaniz-Álvarez, S.A., Ortega-Gutiérrez, F., 1997, Geología y Petrología del Complejo Xolapa en la Barranca de Xolapa, Estado de Guerrero: Boletín de Mineralogía, 13(1), 3-32.

Black, L.P., Kamo, S.L., Allen, C. M., Davis, D.W., Aleinikoff, J.N., Valley, J.W., Mundil, R., Campbell, I.H., Korsch, R.J., Williams, I.S., Foudoulis, C., 2004, Improved $^{206}Pb/^{238}U$ microprobe geochronology by the monitoring of a trace-element-related matrix effect; SHRIMP, ID–TIMS, ELA–ICP–MS and oxygen isotope documentation for a series of zircon standards: Chemical Geology, 205, 115-140.

Brown, E.H., 1996, High-pressure metamorphism caused by magma loading in Fiordland, New Zealand: Journal of Metamorphic Geology, 14, 441-452.

Brown, M., 2004, Melt extraction from lower continental crust: Transactions of the Royal Society of Edinburgh, Earth Sciences, 95, 35–48.

Brown, M., 2005, Melt extraction from the lower continental crust of orogens: the field evidence, *in* Brown, M., Rushmer, T. (eds.), Evolution and Differentiation of the Continental Crust: United Kingdom, Cambridge University Press, 331-383.

Brueckner, H.K., Hamming, S., Sorensen, S.S., Harlow, G.E., 2005, Synchronous Sm-Nd mineral ages from HP terranes on both sides of the Motagua fault of Guatemala: convergent suture and strike-slip fault?, *in* American Geophysical Union, Fall Meeting, San Francisco, California: Eos Transactions AGU, 86(52), Fall Meeting Supplement, abstract T23D-04.

Burckhardt, C., 1927, Cefalópodos del Jurásico Medio de Oaxaca y Guerrero: Universidad Nacional Autónoma de México, Instituto de Geología, Boletín, 47, 108 p.

Campa, M.F., Coney, P.J., 1983, Tectono-stratigraphic terranes and mineral resource distributions in Mexico: Canadian Journal of Earth Sciences, 20, 1040-1051.

Centeno-García, E., Ruíz, J., Coney, P.J., Patchett, P.J., Ortega-Gutiérrez, F., 1993, Guerrero terrane of Mexico: its role in the Southern Cordillera from new geochemical data: Geology, 21, 419-422.

Centeno-García, E., Guerrero-Suastegui, M.,Talavera-Mendoza, O., 2008, The Guerrero Composite Terrane of western Mexico: collision and subsequent rifting in a supra-subduction zone, *in* Draut, A.E., Clift, P.D., Scholl, D.W., Formation and Applications of the Sedimentary Record in Arc Collision Zones: Boulder, Colorado, Geological Society of America, Special Paper, 436, 279-308.

Cerca, M., Ferrari, L., López-Martínez, M., Martiny, B., Iriondo, A., 2007, Late Cretaceous shortening and early Tertiary shearing in the Central Sierra Madre del Sur, southern Mexico: insights into the evolution of the Caribbean - North America plate interaction: Tectonics, 26, TC3007, doi: 10.1029/2006TC001981.

Connelly, J.N., 2001, Degree of preservation of igneous zonation in zircon as a signpost for concordancy in U/Pb geochronology: Chemical Geology, 172, 25-39.

Corfu, F., Hanchar, J.M., Hoskin, P.W.O., Kinny, P., 2003, Atlas of zircon textures, *in* Hanchar, J.M., Hoskin, P.W.O. (eds.), Zircon: Washington D.C., Mineralogical Society of America, Reviews in Mineralogy and Geochemistry, 23, 469-500.

Corona-Chávez, P., Poli, S., Bigioggero, B., 2006, Syn-deformational migmatites and magmatic-arc metamorphism in the Xolapa Complex, southern Mexico: Journal of Metamorphic Geology, 24(3), 169-191, doi:10.1111/j.1525-1314.2006.00632.x.

Corona-Esquivel, R., 1981, Estratigrafía de la región de Olinalá-Tecocoyunca, noreste del Estado de Guerrero: Universidad Autónoma de México, Revista del Instituto de Geología, 5(1), 17-24.

De Cserna, Z., 1965, Reconocimiento geológico de la Sierra Madre del Sur de México, entre Chilpancingo y Acapulco, Estado de Guerrero: Universidad Nacional Autónoma de México, Instituto de Geología, Boletín, 62, 77 p.

Dickinson, W.R., Lawton, T.F., 2001, Carboniferous to Cretaceous assembly and fragmentation of Mexico: Geological Society of America Bulletin, 113(9), 1142-1160.

Ducea, M., Gehrels, G.E., Shoemaker, S., Ruíz, J., Valencia, V.A., 2004, Geologic evolution of the Xolapa Complex, southern Mexico: Evidence from U-Pb zircon geochronology: Geological Society of America Bulletin, 116(7/8), 1016-1025.

Ducea, M., Valencia, V.A., Shoemaker, S., Reiners, P.W., DeCelles, P.G., Campa-Uranga, M.F., Morán Zenteno, D.J., Ruíz, J., 2005, Rates of sediment recycling beneath the Acapulco trench: Constraints from (U-Th)//He thermochronology: Journal of Geophysical Research, 109, doi: 10.1029/2004JB003112.

Elías-Herrera, M., Ortega-Gutiérrez, F., 1998, The Early Cretaceous Arperos oceanic basin (Wester Mexico). Geochemical evidence for an aseismic ridge formed near a spreading center - Comment: Tectonophysics, 292, 321-326.

Elías-Herrera, M., Ortega-Gutiérrez, F., 2002, The Caltepec Fault Zone: an Early Permian dextral transpressional boundary between the Proterozoic Oaxacan and Palaeozoic Acatlán complexes, southern México, and regional tectonic implications: Tectonics, 21(3), 1013, 10.1029/2000TC001278.

Elías-Herrera, M., Sánchez-Zavala, J.L., Macías-Romo, C., 2000, Geologic and geochronologic data from the Guerrero terrane in the Tejupilco area, southern México: new constraints on its tectonic interpretation: Journal of South American Earth Sciences, 13, 355-375.

Elliott, T., Plank, T., Zindler, A., White, W., Bourdon, B., 1997, Element transport from slab to volcanic front at the Mariana arc: Journal of Geophysical Research, 102, 14991-15019.

Gradstein, F.M., Ogg, J.G., Smith, A.G., Bleeker, W., Lourens, L.J., 2004, A new geological time scale, with special reference to Precambrian and Neogene: Episodes, 27(2), 83-100.

Grajales-Nishimura, J.M., 1988, Geology, geochronology, geochemistry and tectonic implications of the Juchatengo green rock sequence, State of Oaxaca, southern México: University of Arizona, M. Sc. thesis, 145 p.

Grajales-Nishimura, J.M., Centeno-García, E., Keppie, J.D.,Dostal, J., 1999, Geochemistry of Paleozoic basalts from the Juchatengo complex of southern Mexico: tectonic implications: Journal of South American Earth Sciences, 12, 537-544.

Guerrero-García, J., Silver, L.T., Anderson, T.H., 1978, Estudios geocronológicos en el Complejo Xolapa: Boletín de la Sociedad Geológica Mexicana, 39, 22-23.

Harlow, G.E., Hemming, S.R., Avé Lallemant, H.G., Sisson, V.B., Sorensen, S.S., 2004, Two high-pressure–low-temperature serpentinite-matrix mélange belts, Motagua fault zone, Guatemala: A record of Aptian and Maastrichtian collisions: Geology, 32(1), 17-20.

Hernández-Pineda, G.A., 2006, Geocronología y geoquímica de granitoides en el área de Tierra Colorada, Guerrero: Mexico, Universidad Nacional Autónoma de México, tesis de Licenciatura, 85 p.

Herrmann, U.R., 1994, The origin of a "terrane": U/Pb zircon systematics, geochemistry and tectonics of the Xolapa Complex (Southern Mexico): Tübingen, Germany, Universität Tübingen, Institut und Museum für Geologie und Palaäontologie, Ph.D. thesis, 92 p.

Herrmann, U., Nelson, B.K., Ratschbacher, L., 1994, The origin of a terrane: U/Pb zircon geochronology and tectonic evolution of the Xolapa complex (southern Mexico): Tectonics, 13(2), 455-474.

Horne, G.S., Clark, G.S.,Pushkar, P., 1976, Pre-Cretaceous rocks of northwestern Honduras: Basement terrane in Sierra de Omoa: American Association of Petroleum Geologists Bulletin, 60, 566-583.

Keppie, J.D., 2004, Terranes of Mexico revisited: A 1.3 billion year odyssey: International Geology Review, 46, 765-794.

Keppie, J.D., Dostal, J., 2001, Evaluation of the Baja controversy using paleomagnetic and faunal data, plume magmatism, and piercing points: Tectonophysics, 339(3-4), 427-442.

Keppie, J.D., Dostal, J., Ortega-Gutiérrez, F., Lopez, R., 2001, A Grenvillian arc on the margin of Amazonia: evidence from the southern Oaxacan Complex, southern Mexico: Precambrian Research, 112, 165-181.

Keppie, J.D., Dostal, J., Cameron, K.L., Solari, L.A., Ortega-Gutiérrez, F., Lopez, R., 2003, Geochronology and geochemistry of Grenvillian igneous suites in the northern Oaxacan Complex, southern Mexico: tectonic implications: Precambrian Research, 120, 365-389.

Keppie, J.D., Nance, R.D., Powell, J.T., Mumma, S.A., Dostal, J., Fox,

D., Muise, J., Ortega-Rivera, A., Miller, B.V.,Lee, J.W.K., 2004, Mid-Jurassic tectonothermal event superposed on a Paleozoic geological record in the Acatlán Complex of southern Mexico: hotspot activity during the breakup of Pangea: Gondwana Research, 7, 239-260.

Keppie, JD, Dostal, J., Murphy, JB, Nance, RD, 2008, Synthesis and tectonic interpretation of the westernmost Paleozoic Variscan orogen in southern Mexico: From rifted Rheic margin to active Pacific margin: Tectonophysics, 461, 277 – 290.

Langmuir, C., Hanson, G., 1980, An evaluation of major element heterogeneity in the mantle sources of basalts: Philosophical Transactions of the Royal Society of London, Series A, 297, 383-407.

Lawlor, P., Ortega-Gutiérrez, F., Cameron, K., Ochoa-Camarillo, H., López, R., Sampson, D., 1999, U/Pb Geochronology, geochemistry and provenance of the Grenvillian Huiznopala Gneiss of eastern Mexico: Precambrian Research, 94, 73-99.

Lehnert, K., Su, Y., Langmuir, C., Sarbas, B. , Nohl, U., 2000, A global geochemical database structure for rocks: Geochemistry, Geophysics, Geosystems, 1(5), 1012, doi:10.1029/1999GC000026.

Levresse, G., González-Partida, E., Carrillo-Chávez, A., Tritlla, J., Camprubí, A., Cheilletz, A., Gasquet, D., Deloule, E., 2004, Petrology, U/Pb dating and (C-O) stable isotope constraints on the source and evolution of the adakite-related Mezcala Fe-Au skarn district, Guerrero, Mexico: Mineralium Deposita, 39, 301-312.

Ludwig, K.R., 2001, SQUID 1.03 –a user's manual: Berkeley, CA, Berkeley Geochronology Center, Special Publication 2, 19 pp.

Ludwig, K.R., 2004, Isoplot/Ex, ver. 3, A geochronological toolkit for Microsoft Excel: Berkeley Geochronology Center, Special Publication 4, 70 pp.

Martens, U., Solari, L.A., Sisson, V.B., Harlow, G.E., Torres de León, R., Ligorria, J.P., Tsujimori, T., Ortega-Gutiérrez, F., Brueckner, H.K., Giunta, G., Avé Lallemant, H.G., 2007, High-pressure belts of central Guatemala: The Motagua suture and the Chuacús Complex, Field Trip Guide, 2007 Field Workshop of IGCP 546 "Subduction Zones of the Caribbean": Guatemala City, 32 p.

McDonough, W., Sun, S., 1995, The composition of the earth: Chemical Geology, 120, 223-253.

Mehnert, K.R., 1968, Migmatites and the origin of granitic rocks: Amsterdam, Elsevier, 393 p.

Meschede, M., Frisch, W., Herrmann, U., Ratschbacher, L., 1997, Stress transmission across an active plate boundary: an example from southern Mexico: Tectonophysics, 266, 81-100.

Milord, I., Sawyer, E.W., 2003, Schlieren formation in diatexite migmatite: examples from the St Malo migmatite terrane, France: Journal of Metmorphic Geology, 21, 347-362.

Morán-Zenteno, D.J., 1992, Investigaciones isotópicas de Rb-Sr y Sm-Nd en rocas cristalinas de la región Tierra Colorada - Acapulco - Cruz Grande, Estado de Guerrero: México, Universidad Autónoma de México, Ph. D. thesis 186 p.

Morán-Zenteno, D.J., Corona-Chávez, P., Tolson, G., 1996, Uplift and subduction erosion in southwestern Mexico since the Oligocene: pluton geobarometry constraints: Earth and Planetary Science Letters, 141, 51-65.

Morán-Zenteno, D.J., Tolson, G., Martínez-Serrano, R.G., Martiny, B., Schaaf, P., Silva-Romo, G., Macías-Romo, C., Alba-Aldave, L., Hernández-Bernal, M.S., Solís-Pichardo, G., 1999, Tertiary arc-magmatism of the Sierra Madre del Sur, Mexico, and its transition to the volcanic activity of the Trans-Mexican Volcanic Belt: Journal of South American Earth Sciences, 12, 513-535.

Morán-Zenteno, D.J., Cerca-Martínez, M., Keppie, J.D., 2005, La evolución tectónica y magmática cenozoica del suroeste de México: avances y problemas de interpretación: Boletín de la Sociedad Geológica Mexicana, 57(3), 319-341.

Nourse, J.A., Premo, W.R., Iriondo, A., Stahl, E.R., 2005, Contrasting Proterozoic basement complexes near the truncated margin of Laurentia, northwestern Sonora-Arizona international border region, *in* Anderson, T.H., Nourse, J.A., McKee, J.W., Steiner, M.B.(eds.), The Mojave-Sonora Megashear Hypothesis: Development, Assessment, and Alternatives: Boulder, Colorado, Geological Society of America Special Paper, 393, 123-182.

Ortega-Gutiérrez, F., Elías-Herrera, M., 2003, Wholesale melting of the southern Mixteco terrane and origin of the Xolapa Complex (abstract) *in* Geological Society of America, Cordilleran Section, 99th annual meeting, Puerto Vallarta, Jal., Mexico: Geological Society of America, Abstracts whit programs, paper 27-6.

Ortega-Gutiérrez, F., Elías-Herrera,M., Reyes-Salas, M., Macías-Romo, C., Lopez, R., 1999, Late Ordovician - Early Silurian continental collision orogeny in southern Mexico and its bearing on Gondwana - Laurentia connections: Geology, 27, 719-722.

Ortega-Gutiérrez, F., Solari, L.A., Ortega-Obregón, C., Elías-Herrera, M., Martens, U., Morán-Icál, S., Chiquín, M., Keppie, J.D., Torres de León, R., Schaaf, P., 2007, The Maya-Chortís boundary: a tectonostratigraphic approach: International Geology Review, 49, 996-1024.

Pearce, J.A., Harris, N.B.W., and Tindle, A.G., 1984, Trace element discrimination diagrams for the tectonic interpretation of granitic rocks: Journal of Petrology, 25, 956–983.

Pérez-Gutiérrez, R., 2005, Geología y evolución estructural del Complejo Xolapa, entre los Ríos Papagayo y La Sábana, noreste de Acapulco: Guerrero, Mexico, Universidad Nacional Autonoma de México, Posgrado en Ciencias de la Tierra, M. Sc. thesis, 80 p.

Riller, U., Ratschbacher, L., Frisch, W., 1992, Left-lateral transtension along the Tierra Colorada deformation zone, northern margin of the Xolapa magmatic arc of southern Mexico: Journal of South American Earth Sciences, 5(3-4), 237-249.

Robinson, K.L., Gastil, G.R., Campa, M.F., 1989, Early Tertiary extension in southwestern Mexico and the exhumation of the Xolapa metamorphic core complex *in* Geological Society of America, Annual Meeting: Geological Society of America, Abstracts with Programs, p. A92.

Sabanero-Sosa, H., 1990, La ruptura del extremo austral de la plataforma Guerrero-Morelos determinada por la accreción contructiva-transformante del Terreno Xolapa: México, Instituto Politécnico Nacional, Tesis de Licenciatura, 126 p.

Schaaf, P., Morán-Zenteno, D.J., Hernández-Bernal, M.S., Solís-Pichardo, G., Tolson, G., Kohler, H., 1995, Paleogene continental margin truncation in Southwestern México: Geochronological evidence: Tectonics, 14(5), 1339-1350.

Schaaf, P., Stimac, J., Siebe, C., Macías, J., 2005, Geochemical evidence for mantle origin and crustal processes in volcanic rocks from Popocatépetl and surrounding monogenetic volcanoes, Central Mexico: Journal of Petrology, 46, 1243-1282.

Schwartz, D.P., 1977, Geology of the Zacapa Quadrangle and vicinity, Guatemala, Central America: USA, State University of New York at Binghamton, Ph. D. thesis, 191 p.

Sedlock, R.L., Ortega-Gutiérrez, F., Speed, R. C., 1993, Tectonostratigraphic terranes and tectonic evolution of Mexico: Geological Society of America Special Paper 278, 153 pp.

Solari, L.A., Keppie, J.D., Ortega-Gutiérrez, F., Cameron, K.L., Lopez, R., Hames, W.E., 2003, Grenvillian tectonothernmal events in the northern Oaxacan Complex, southern Mexico: roots of an orogen: Tectonophysics, 365, 257-282.

Solari, L.A., Keppie, J.D., Ortega-Gutiérrez, F., Cameron, K.L., Lopez, R., 2004, ~ 990 Ma peak granulitic metamorphism and amalgamation of Oaxaquia, Mexico: U-Pb zircon geochronological and common Pb isotopic data: Revista Mexicana de Ciencias Geológicas, 21(2), 212-225.

Solari, L.A., Torres de León, R., Hernández-Pineda, G.A., Solé, J., Hernández-Treviño, T., Solís-Pichardo, G., 2007, Tectonic significance of Cretaceous–Tertiary magmatic and structural evolution of the northern margin of the Xolapa Complex, Tierra Colorada area, southern Mexico: Geological Society of America Bulletin, 119(9/10), 1265-1279.

Solé, J., 2004, Descifrando los eventos tectonotérmicos cenozoicos en el norte del Complejo Xolapa entre Tierra Colorada y Acapulco (México) mediante geocronología de K-Ar (abstract), *in* IV Reunión Nacional de Ciencias de la Tierra, Juriquilla, Querétaro, Libro de resúmenes, SE03-7.

Sun, S., McDonough, W., 1989, Chemical and isotopic systematics of oceanic basalts: Implications for mantle compositions and processes,

in Saunders, A., Norry, M. (eds.), Magmatism in the Ocean Basins: Geological Society Special Publication 42, 313-345.

Talavera-Mendoza, O., Ruíz, J., Gehrels, G.E., Valencia, V.A., Centeno-García, E., 2007, Detrital zircon U/Pb geochronology of southern Guerrero and western Mixteca arc successions (southern Mexico): New insights for the tectonic evolution of southwestern North America during the late Mesozoic: Geological Society of America Bulletin, 119(9/10), 1052-1065.

Tolson, G., 2005, La falla Chacalapa en el sur de Oaxaca: Boletín de la Sociedad Geológica Mexicana, 57(1), 111-122.

Torres-de León, R., 2005, Análisis Estructural y Caracterización Petrográfica de Unidades Miloníticas en el Área de La Venta, Estado de Guerrero: Implicaciones Tectónicas: Universidad Nacional Autónoma de México, Posgrado en Ciencias de la Tierra, Master tesis, 65 p.

Warren, R.G., Ellis, D. J., 1996, Mantle underplating, granite tectonics, and metamorphic P-T-t paths: Geology, 24(7), 663-666.

Weber, B., Schaaf, P., Valencia, V.A., Iriondo, A., Ortega-Gutiérrez, F., 2006, Provenance ages of late Paleozoic sandstones (Santa Rosa Formation) from the Maya block, SE Mexico. Implications on the tectonic evolution of western Pangea: Revista Mexicana de Ciencias Geológicas, 23(2), 262-276.

Whitney, D.L., Miller, R.B., Paterson, R., 1999, P-T-t evidence for mechanisms of vertical motion in a contractional orogen: northwestern US and Canadian Cordillera: Journal of Metamorphic Geology, 17, 75-90.

Yañez, P., Ruíz, J., Patchett, P.J., Ortega-Gutiérrez, F., Gehrels, G.E., 1991, Isotopic studies of the Acatlan Complex, southern Mexico: Implications for paleozoic North American tectonics: Geological Society of America Bulletin, 103, 817-828.

Manuscript received: January 22, 2008
Corrected manuscript accepted: August 13, 2008
Manuscript accepted: September 9, 2008